1997MNRAS.286....1P

Mon. Not. R. Astron. Soc. **286,** 1–22 (1997)

RV Tauri stars – II. A spectroscopic study

Karen R. Pollard,[1,2★] P. L. Cottrell,[2★] W. A. Lawson,[3★] Michael D. Albrow[2★†] and W. Tobin[2★]

[1]*South African Astronomical Observatory, PO Box 9, Observatory 7935, South Africa*
[2]*Mount John University Observatory, Department of Physics and Astronomy, University of Canterbury, Private Bag 4800, Christchurch, New Zealand*
[3]*Australian Defence Force Academy, Department of Physics, University of New South Wales, Canberra, ACT 2600, Australia*

Accepted 1996 September 14. Received 1996 September 9; in original form 1996 April 11

ABSTRACT

A long-term photometric and spectroscopic survey of eleven RV Tauri stars has been undertaken with a view to obtaining a better understanding of the nature of these pulsating variables. Pollard et al. presented the results from the long-term multicolour photometric survey. This paper presents the contemporaneous moderate- to high-resolution spectroscopy of these stars.

All the RV Tauri stars in our sample display, or are consistent with, two shock waves propagating in their atmospheres per 'formal' period (the time between successive deep minima). This is consistent with the few previous high-resolution spectroscopic studies of the three brightest RV Tauri stars: R Sct, U Mon and AC Her.

Specifically, the Hα profiles exhibit two enhancements of emission per cycle following the passage of the primary and secondary shock waves through the photosphere around phases 0.1 and 0.6. Metallic lines showed 'doubled' profiles characteristic of an atmospheric shock wave around these phases, with evidence of two radial velocity cycles per formal period.

In the RVb-type stars, an additional contribution to the Hα emission is seen and this appears to be correlated with the long-term period. Two stars, AI Sco and IW Car, display extended blueward Hα absorption which may arise from mass outflow. Evidence of long-term radial velocity variations is also seen in a number of the RVb stars.

Key words: stars: AGB and post-AGB – stars: oscillations – stars: variables: other.

1 INTRODUCTION

The RV Tauri variables occupy a region of the Hertzsprung–Russell diagram that is populated by a large variety of evolved luminous variable stars. A knowledge of the spectroscopic properties of the RV Tauri stars is an important step towards a better understanding of their evolutionary status and the possible relationship between these objects and adjacent groups of variables such as the classical and type II Cepheids (Pollard et al.1996b), R Coronae Borealis stars, SRd stars, long-period variables and post-AGB-type objects. The evolutionary status of the RV Tauri stars is rather uncertain and any clues as to possible progenitors or future evolution are extremely valuable.

Some of the more striking spectral peculiarities of the RV Tauri stars are the presence of strong emission in the Balmer and metallic lines and the doubling of some absorption lines at particular pulsational phases. As discussed by Wallerstein & Cox (1984), these features provide strong evidence that shock waves are present in the atmospheres of these stars. In addition, the appearance of TiO absorption bands in many RV Tauri stars, in some cases as strong as in an M5-type star, indicate that the physical conditions are substantially different from those in more 'normal' stars.

1.1 Previous spectroscopic studies of the RV Tauri variables

There are a number of general spectroscopic surveys of the RV Tauri class of variables. The low-resolution studies by Rosino (1951) and Joy (1952) looked at the spectra and radial velocities of the RV Tauri and semiregular stars in an attempt to assign population types and define subgroups with well-defined properties and behaviour. In both surveys the same general trends were noted: high or very high luminosities (Ib or Ia), hydrogen emission lines apparent during increasing light, latest spectral types (about K0) occurring close to the deep light minima, the maximum excitation and earliest spectral types (about G0) occurring just before primary maxima and TiO bands appearing in some stars near the deep minima. One of the main conclusions reached was that the RV Tauri stars do not form a homogeneous group.

The spectroscopic subclassification scheme that has generally been adopted is the one described by Preston et al. (1963). In this scheme the RV Tauri stars are divided into three subtypes: Preston

★E-mail: krp@saao.ac.za (KRP); p.cottrell@csc.canterbury.ac.nz (PLC); wal@phadfa.ph.adfa.oz.au (WAL); m.albrow@csc.canterbury.ac.nz (MDA); w.tobin@csc.canterbury.ac.nz (WT)
†Visiting Astronomer, South African Astronomical Observatory.

© 1997 RAS

© Royal Astronomical Society • Provided by the NASA Astrophysics Data System

1997MNRAS.286....1P

Table 1. Summary of RV Tauri spectroscopic observations.

Star	Preston type[b]	MJUO spectra N	MJUO spectra Exp (min)	MSSSO spectra N	MSSSO spectra Exp (min)	Photometric ephemeris[a] Zero Point (2440000+)	Photometric ephemeris[a] Period (d)	Previous spectroscopic studies Spectral range	Previous spectroscopic studies Radial Velocity ($km\,s^{-1}$)
RVa photometric subclass									
R Sct	A	27	15–30	19	2–5	8073.05	140.30	G5Iae–K2p(M3)Ibe[c]	+24.8 to +56.6[d]
AR Sgr	A	4	60	11	10	8362.57	88.86	F5e–G6[c]	−108 to −88[c]
RU Cen	B	14	60	15	5–10	8124.57	64.60	A7Ib–G2pe[e], G2–K2[f]	–
AD Aql	B	0	–	11	10–15	8086.84	66.09	Fp(R)[b]	–
V453 Oph	C	0	–	2	10	8340.55	80.68	Fp[b]	−95[g]
RY Ara	A?	8	60	12	5–10	8315.6	289.6	G5–K0[e]	–
V820 Cen	–	13	60	14	5–10	8338.7	159.4	K0e[e]	+258[h], +261[i]
RVb photometric subclass									
U Mon	A	29	15–30	8	2–5	8130.00	92.32	F8eIb–K0p(M2)Ib[c]	−2 to +62[j]
AI Sco	A	1	60	9	4–10	8373.93	71.03	G0–K2[c]	−40 to −3[c]
AR Pup	B	10	60	9	5–10	8071.09	77.79	cF0–cF8[k], Rp[f]	–
IW Car	B	22	40–60	13	3–15	8123.0	72.0	F7/F8[l]	–

[a]Pollard et al. (1996a); [b]Preston et al. (1963); [c]Joy (1952); [d]Preston (1962); [e]Kholopov et al. (1985); [f]Rosino (1951); [g]Joy (1950); [h] Wegner (1976); [i]Hunger & Kaufmann (1976); [j] Preston (1964); [k]Payne-Gaposchkin, Brenton & Gaposchkin (1943); [l]Houk (1978).

type A (G–K type variables with TiO bands sometimes occurring at minimum light); Preston type B [Fp(R) variables which show evidence of enhanced carbon]; and Preston type C (Fp variables, to which subclass the globular cluster variables generally belong).

Using high-resolution spectroscopy and CORAVEL velocities obtained over several pulsation cycles of R Sct, Gillet et al. (1989) and Gillet, Burki & Duquennoy (1990) showed the existence of two shock waves and their associated accelerations within the atmosphere during each luminosity period (~140 d). High-resolution spectroscopy of pure photospheric absorption Fe I lines by Lèbre & Gillet (1991a) confirmed the presence of two acceleration peaks per luminosity period. This latter study found that large outward accelerations and strong Hα emission were associated with each shock wave. However, their finding that Fe I lines of similar excitation potential display very large variations in the velocity amplitude is undoubtedly due to the fact that they have mistakenly used ΔE ($= E_{\rm upper} - E_{\rm lower}$ = energy of transition) as the value of the excitation potential. Consequently, the Fe I lines that they used (in the region 6550–6620 Å) have almost exactly the same 'excitation potential' of 1.87–1.89 eV. In reality, their pure absorption Fe I lines have excitation potentials of between 1.01 and 4.79 eV and thus large variations in the velocity amplitude (due to quite different depths of formation of these Fe I lines) are not unexpected. Lèbre & Gillet (1991a) found that the acceleration in R Sct was strongest around phase 0.0 corresponding to the primary and strongest shock, whereas the earlier paper using CORAVEL velocities (Gillet et al. 1990) found that the secondary shock was the strongest in both AC Her and R Sct.

Mozurkewich et al. (1987) studied the velocity structure of R Sct using high-resolution 2-μm Fourier-transform spectrograms obtained at different pulsational phases. The high-excitation atomic absorption lines, which form in deep photospheric layers, display a continuous repeatable pulsation with a period of about 142 d. This result did not appear to be consistent with previous optical studies which showed a 70-d period and a discontinuous velocity curve.

In this paper we present the results of a long-term study into the spectroscopic properties and behaviour of the RV Tauri stars. Moderate- to high-resolution spectra of eleven stars classified as RV Tauri type [and with a range of Preston et al. (1963) spectroscopic subtypes, see Table 1] were used to investigate the radial velocity variations, the stratification and structure of the atmospheres and the effects of shock waves. In Section 2 we present a brief description of the spectroscopic observations and the techniques employed to reduce and analyse them. The results of the RV Tauri spectroscopic programme are presented in Section 3. Finally, in Section 4, we summarize these results and discuss them with reference to various pulsational models.

2 OBSERVATIONS AND ANALYSIS TECHNIQUES

2.1 Observations

Moderate- to high-resolution spectra of eleven variables classified as RV Tauri stars have been obtained using the 1.0-m reflector at the Mount John University Observatory (MJUO) and the 1.9-m reflector at the Mount Stromlo and Siding Spring Observatories (MSSSO).

Echelle spectra of nine stars were obtained at MJUO between 1991 January and1992 September. Observations of the two brightest RV Tauri stars, R Sct and U Mon, were continued until 1994 April. The echelle spectrograph was used in conjunction with a Photometrics 3000 CCD camera system (incorporating a 384×576 pixel Thomson CCD chip) to observe three different wavelength regions. Two regions in the red sample approximately 30 Å of each of four orders (including the Hα line and the 6707-Å Li I line), while the 'Na region' samples about 30 Å of each of five orders (including the Na D lines). Because of this short wavelength coverage, the MJUO spectra are not as useful as the MSSSO spectra in showing shallow extended absorption or emission features. The reciprocal dispersion of the MJUO echelle spectrograph is 2 Å mm^{-1} at Hα, corresponding to a resolving power of $R \sim 30\,000$. The MJUO spectra were reduced using modified echelle reduction routines within the MIDAS software package. Wavelength calibration uncertainties are typically less than 0.002 Å, corresponding to 0.1 $km\,s^{-1}$. Observations of IAU standard stars have shown that the MJUO radial velocities are consistent with the absolute (IAU) radial velocity system to better than ±1.0 $km\,s^{-1}$.

© Royal Astronomical Society • Provided by the NASA Astrophysics Data System

1997MNRAS.286....1P

Spectroscopic observations of eleven RV Tauri stars were obtained at MSSSO between 1991 May and 1991 September using the coudé spectrograph and GEC CCD detectors. Between 100 and 200 Å of the region around the Hα line was observed. The 82-cm camera and 600 line mm^{-1} 'C' grating in the second order gave a reciprocal dispersion of 10 Å mm^{-1}. A slit width of typically 300 μm was used, equivalent to 1.2 arcsec on the sky, 3-pixel resolution and a resolving power of $R \sim 13\,000$. The MSSSO spectra were reduced using standard library routines within the IRAF software package (see Lawson et al. 1993). The typical wavelength calibration uncertainty of 0.005 Å corresponds to a random error of $\sim 0.3\,km\,s^{-1}$. Observations of three IAU radial velocity standard stars (β CrV, β Oph and δ Sgr) were also obtained throughout the MSSSO observing runs. These observations were used to determine the radial velocity zero-point shifts between different observing runs and to convert the MSSSO radial velocities to absolute (IAU) radial velocities. The mean standard deviation of the corrected standard star velocity residuals was used as an estimate of the standard error in the radial velocities. This was calculated to be $1.3\,km\,s^{-1}$.

Table 1 presents a summary of the spectroscopic observations from MJUO and MSSSO. The phases at which the RV Tauri spectra were obtained were calculated using the ephemerides derived from the photometric analyses (Pollard et al. 1996a), where phase 0.0 defines the time of the primary *V* minima. A summary of results from previous spectroscopic studies is included in this table.

2.2 Measuring metallic radial velocities

The line bisector method (Wallerstein et al. 1992; Albrow 1994) was used to calculate the radial velocities of the metallic lines when these lines were clean and unaffected by shock-related emission or line doubling. In this method, the continuum is designated as being at depth 0.0 and the core of the spectral line at depth 1.0. The wavelength of the bisector is determined at specific fractions (0.5, 0.6, 0.7, 0.8 and 0.9) of the line depth. Depths of less than 0.5 and greater than depth 0.9 are not used, owing to possible contamination from neighbouring spectral lines and limits on the algorithm close to depth 1.0 respectively. The corresponding radial velocities at the various depths in the line profile are calculated from the relative shift of the line from its rest wavelength. The average over the velocities derived at depths 0.7, 0.8 and 0.9 is used to produce the radial velocity curves for a particular spectral line from the reduced MJUO and MSSSO spectra.

During the phases when shock-related line doubling is present, the metallic lines are fitted by two Gaussian components in order to reproduce the total line profile at that particular phase. For this purpose the Gaussian fitting program GAUSS, in the software reduction package FIGARO, is used. The position, the height and the full width at half-height of each Gaussian are adjusted interactively until a reasonable fit is obtained. The GAUSS program then optimizes the fit by minimizing the sum of the square of the residuals. The individual fitted Gaussians plus the sum of the Gaussians (the fit to the line profile) are displayed, together with the residuals for the fit. The radial velocities for both components are then calculated from the relative shifts of the Gaussians from the rest wavelength of the line.

3 SPECTROSCOPIC RESULTS

The results for the stars of the RVa photometric subclass are presented first since these do not appear to have long-term radial velocity variations that may complicate the analysis. The stars of the RVb photometric subclass are then discussed.

A qualitative description is given of the appearance and phase-dependent behaviour of the shock-related spectral features, such as Hα emission, doubled metallic absorption lines and metallic emission lines. In order to investigate the phase-dependent behaviour of the Hα emission strength in a more quantitative manner, the equivalent width of the Hα profile was measured and plotted versus phase. A convention was adopted whereby a positive equivalent width indicates an overall absorption contribution and a negative measurement indicates that emission is dominant.

Radial velocities were measured for selected metallic lines. In general we used the the Fe I lines with $\chi \sim 2.5$ eV for the Preston type A stars (G–K types or strong-lined) and the C I line at 6587.622 Å for the Preston type B stars (weak-lined and carbon-enhanced). Table 2 presents a summary of the lines used for the radial velocity measurements, together with their wavelengths and excitation potentials.

Due to their relative brightness, more spectra were obtained of R Sct (RVa subclass) and U Mon (RVb subclass) than of the other stars in the programme. A more detailed discussion and analysis of these stars is presented in Sections 3.1 and 3.8 respectively.

Table 2. The wavelengths (λ) and excitation potentials (χ) of lines used for measuring radial velocities for the RV Tauri stars.

species	λ (Å)	χ (eV)	multiplet
Na I	5889.950	0.00	1
Na I	5895.920	0.00	1
Fe I	6200.321	2.61	207
Fe I	6546.245	2.76	268
H I	6562.808	10.20	1
Fe I	6569.224	4.73	1253
C I	6587.622	8.53	22
S I	6743.575	7.86	8
S I	6748.779	7.87	8
Fe I	6750.164	2.42	111
S I	6757.195	7.87	8

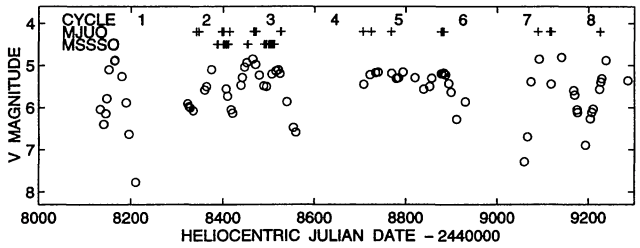


Figure 1. The light curve and spectral phase coverage for R Sct. The MJUO photometric observations (∘) and the times when spectroscopic observations were obtained at both MJUO and MSSSO (+) are shown versus heliocentric Julian Date. The beginning of each new cycle (according to the photometric ephemeris) is also indicated.

3.1 R Sct

The MJUO *V* photometry for R Sct and the dates when spectra were

© Royal Astronomical Society • Provided by the NASA Astrophysics Data System

1997MNRAS.286....1P

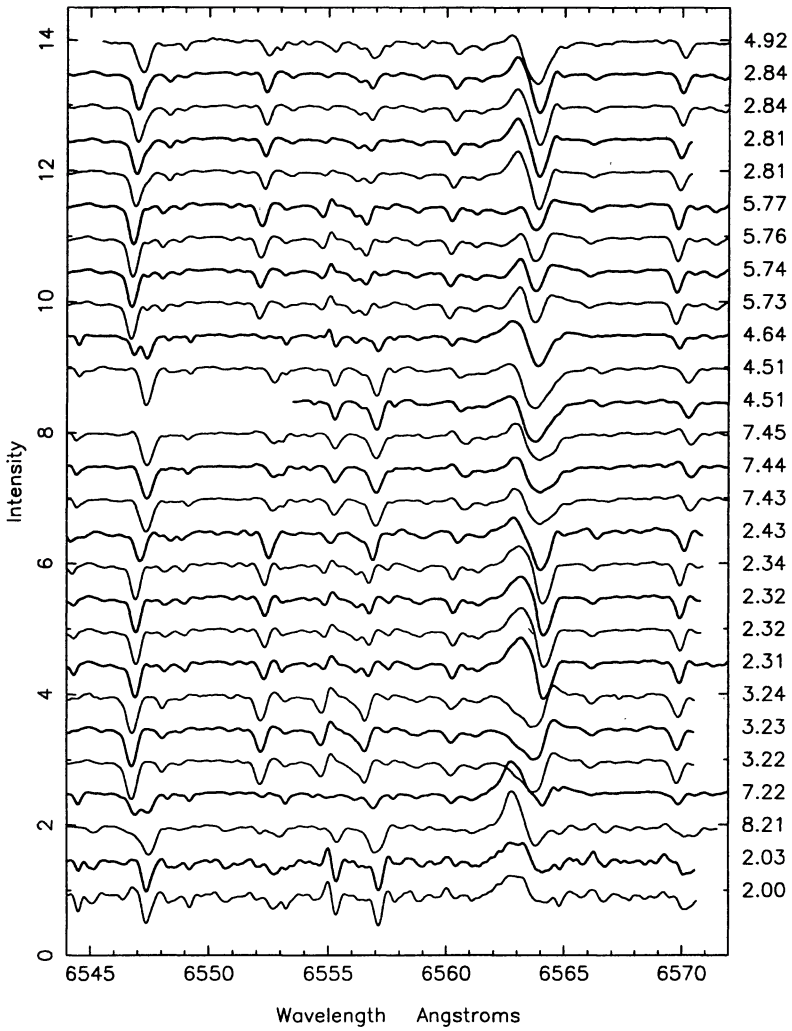


Figure 2. Stacked MJUO spectra of the region around Hα in R Sct. The cycle number and phase are indicated to the right of each spectrum.

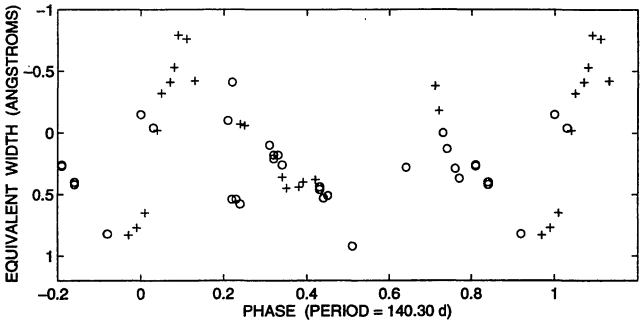


Figure 3. The phase dependence of the Hα emission strength in R Sct from measurements of the Hα equivalent width on the MJUO (∘) and MSSSO (+) spectra.

obtained at MJUO and MSSSO are shown in Fig. 1. Detailed dates, phases and radial velocities are given for R Sct in Table A1. Due to the irregularity of the light variations, some of the phases calculated from the photometric ephemeris are not consistent with the actual MJUO light curve. In these cases, the phases from the MJUO light curve have been adopted.

3.1.1 The Hα line

Sequences of MJUO spectra stacked in phase order (Fig. 2) show evidence of increases in the strength of the Hα emission during phases 0.0–0.3 and 0.5–0.8. This is consistent with previous high-resolution optical studies (Preston 1962; Gillet et al. 1989, 1990; Lèbre & Gillet 1991a) which showed that two shock waves are produced during each 140-d cycle.

The phase dependence of the Hα emission strength is shown in Fig. 3. R Sct shows strong Hα emission (negative equivalent width) just after each light curve minimum around phases 0.1 and 0.7. The emission following the primary light minima is associated with the primary shock wave. This appears to be stronger than the emission associated with the secondary shock which follows the secondary light minima, although fewer spectra were obtained during the secondary minima.

At phase ~0.2 the Hα emission is much less in cycle 3 than in cycles 2, 7 and 8. During cycles 2 and 7–9, R Sct displayed very regular deep–shallow light variations with quite deep (V=7.0–8.0) primary minima, whereas, between cycles 2 and 5, irregular light variations with minima no deeper than $V \sim 6.5$ were observed (see Fig. 1). Consequently, it appears that stronger Hα emission is associated with the deeper and more regular

© Royal Astronomical Society • Provided by the NASA Astrophysics Data System

1997MNRAS.286....1P

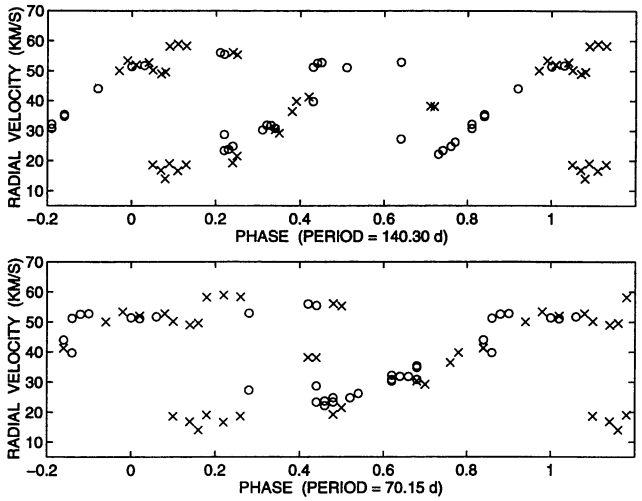


Figure 4. Radial velocity curves for R Sct. The radial velocities for the Fe I line at 6546.245 Å are shown for the MJUO (∘) and the MSSSO spectra (×). The data in the top panel are phased using the 140.30-d 'formal' or photometric period while the data in the bottom panel are phased using the 70.15-d 'fundamental' or dynamic period.

pulsations, as originally suggested in the study by McLaughlin (1938).

3.1.2 The metallic and molecular lines in R Sct

In contrast to the highly variable strength and appearance of the Hα profile, the metallic lines behave in a much more predictable manner. The radial velocities for the Fe I lines at 6546.245, 6569.224 and 6750.164 Å were measured using the line bisector method as described in Section 2.2. Fig. 4 shows that two radial velocity cycles occur during each 140.30-d photometric cycle and a period of 70.15 d may be more fundamental for the radial velocity variations and for the dynamics of the outer envelope. The question of which period is the more intrinsic will be revisited in Section 4. In the following discussion we use the 140.30-d period when calculating the phases.

Around photometric phases 0.1–0.3 and 0.5–0.7, the Fe I lines at 6546.245 and 6750.164 Å display two components, indicating that shock waves are propagating through the regions of the stellar atmosphere where these lines are forming. The phases during which line doubling is present vary slightly from cycle to cycle. The lack of strong line-doubling behaviour in the Fe I line at 6569.224 Å is most likely due to the fact that this line has a higher excitation potential and is therefore expected to form deeper in the atmosphere. The deeper-forming lines should be affected first by the outwardly moving pulsation and affected less by the related shock fronts.

Cycle-to-cycle variations in the radial velocity curve can be seen in Fig. 4. The radial velocities during phases 0.4–0.5 in cycle 7 are much larger (by about 12 km s^{-1}) than those at nearly the same phase but in cycles 2 and 4. Cycle 7 corresponds to when R Sct was pulsating in a more regular manner with much deeper primary minima. It appears that the deeper, more regular pulsations may be correlated with larger velocity amplitudes, although further observations are required to confirm this finding. This also reinforces the need for contemporaneous photometry during spectroscopic campaigns, in order to relate photometric phases to any spectral peculiarities.

The Ti I lines (such as the line at 6554.238 Å) display emission components during phases 0.0–0.35 and 0.55–0.80 which evolve from a P Cygni profile through to an inverse P Cygni type profile (Fig. 2). This sequence of profiles indicates that expanding and infalling layers are simultaneously present in the stellar atmosphere. The Ti I lines which display such strong shock-related behaviour must form higher in the atmosphere than the Fe I lines, and this is consistent with the fact that these features occur slightly later in phase than the Fe I line doubling.

Four spectra of R Sct were obtained of the Na D line region (Fig. 5). The profiles of the two broad stellar Na I lines are complex

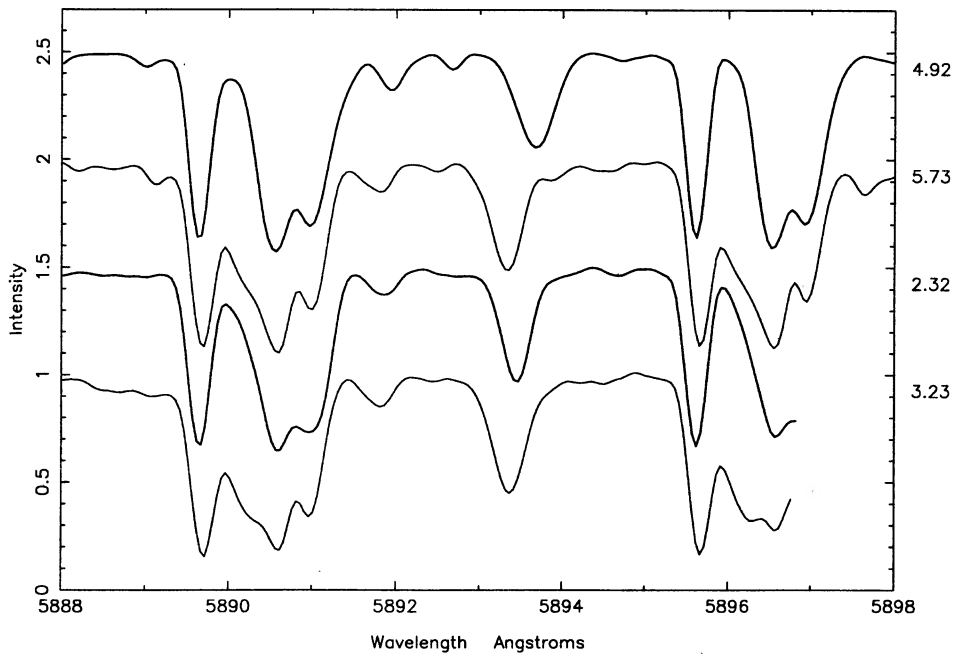


Figure 5. Four MJUO spectra of R Sct showing the complex profiles of the sodium D lines.

© Royal Astronomical Society • Provided by the NASA Astrophysics Data System

1997MNRAS.286....1P

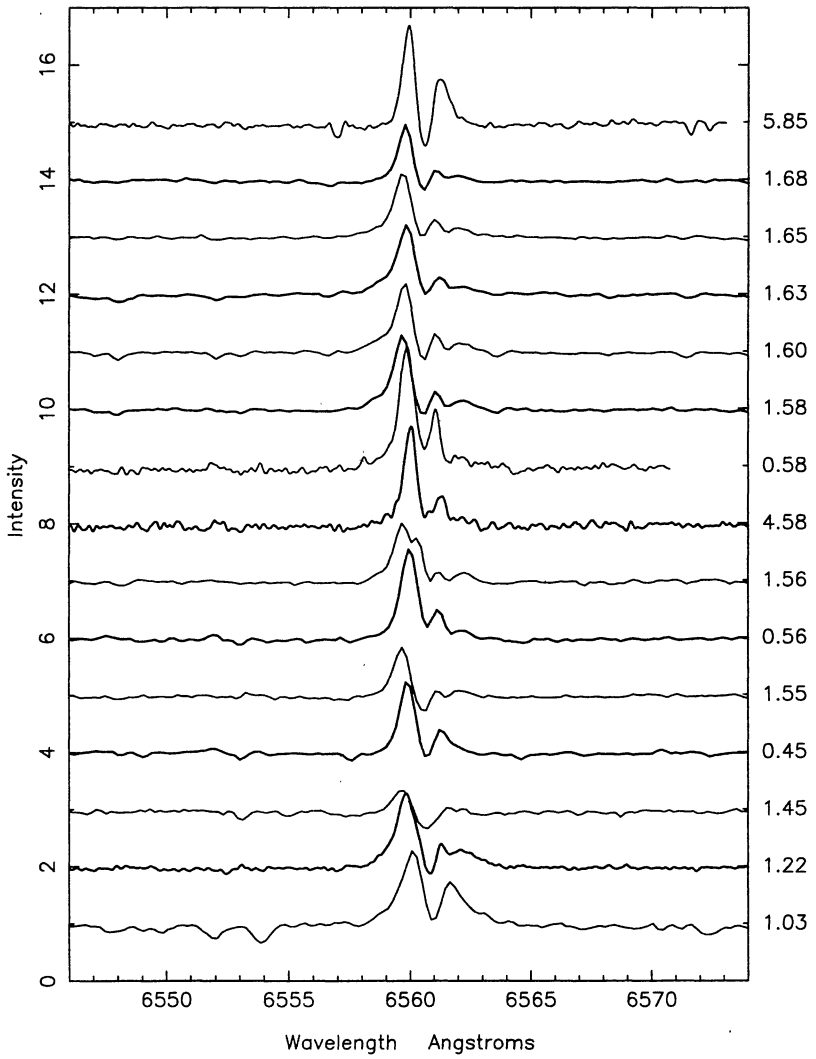


Figure 6. Stacked MJUO and MSSSO spectra of AR Sgr. The cycle number and phase are indicated to the right of each spectrum.

with obvious multiple components. The narrow blueshifted components of the Na I lines are almost stationary, suggesting an interstellar or circumstellar origin.

High-resolution observations of Na I line profiles have been used previously to study the motion of the extended atmosphere in R Sct (Lèbre & Gillet 1991b). These authors suggest that the narrow, blueshifted Na lines may arise in a expanding shell of previously ejected matter. Using radial velocity measurements from their own spectra and those of Luck (1981), Lèbre & Gillet find a velocity decrease in the stellar rest frame ($V_\gamma = 42.1\,\mathrm{km\,s^{-1}}$) from -57.7 ± 0.7 to $-55.1 \pm 0.5\,\mathrm{km\,s^{-1}}$ during the interval from 1977 to 1990.

In order to examine this ejected matter hypothesis, the radial velocities for both narrow, blueshifted Na D components were measured on the two MJUO spectra which displayed lines that were well separated from the stellar sodium lines (phases 2.32 and 4.92). The mean velocity obtained ($-57.6 \pm 0.5\,\mathrm{km\,s^{-1}}$) appears not to support the slow velocity decrease suggested. If the blueshifted component does arise from absorption in matter that has been previously ejected, as proposed by Lèbre & Gillet, then our measurements suggest that the expansion rate of this material is relatively constant.

Molecular lines of TiO and CN are generally strong around the phases of the light minima (phases 0.0 and 0.5). However, the MSSSO spectra at phases 0.0–0.15 from cycle 3 show no evidence of molecular lines, in contrast to the MJUO spectra obtained at the same phases in cycle 2. This is most likely due to the fact that R Sct was pulsating in a rather irregular manner during this time and may have been more extended and cooler during cycle 2.

3.2 AR Sgr

A phase sequence of AR Sgr spectra obtained at MJUO and MSSSO is displayed in Fig. 6. Details of the observations are given in Table A2. The Hα line is very strong, showing multi-peaked emission on many of the spectra. The spectral phase coverage during cycle 1 was relatively good and the Hα equivalent widths from this cycle show an enhancement of the emission around phases 0.1 and 0.6. Large cycle-to-cycle variations in the emission strength are present, e.g. the emission in cycle 0 is much stronger than that in the following cycle.

Metallic absorption lines are strongest at phase 0.03 in cycle 1 and phase 0.85 in cycle 5. Emission components of the 6554.238-Å Ti I line and the 6546.245-Å Fe I line are seen at phases 0.22 and 0.45–0.65. No measurable metallic lines could be found that appeared to be unaffected by the atmospheric shock waves.

© Royal Astronomical Society • Provided by the NASA Astrophysics Data System

1997MNRAS.286....1P

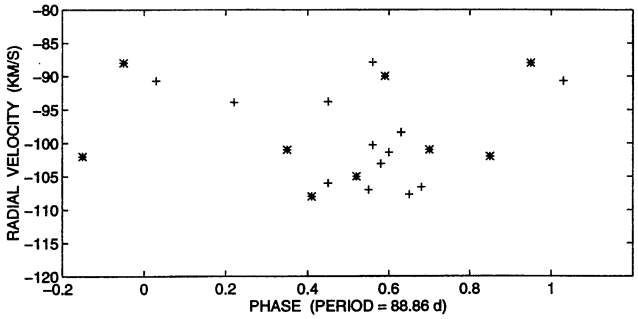


Figure 7. The radial velocities for the Hα absorption component (+) on the MJUO and MSSSO spectra of AR Sgr. Joy's (1952) radial velocities are also shown (∗).

However, radial velocities were measured from fitting Gaussian absorption and emission components to the profile of the Hα line at 6562.808 Å. Fig. 7 shows that the radial velocities of the absorption component are consistent with the presence of two velocity cycles during each 88.86-d photometric cycle (although much cycle-to-cycle scatter is present during phases 0.5–0.7). These Hα absorption velocities are also in good agreement with the radial velocities presented by Joy (1952).

The MSSSO spectrum taken at phase 0.03 in cycle 1 displays very strong molecular bands. At this phase TiO bandheads are seen at 6651.5 and 6681.1 Å and a CN bandhead is apparent at 6631.3 Å. Weak molecular bandheads are also seen on the MSSSO spectrum taken close to secondary minimum at phase 1.45.

3.3 RU Cen

A phase sequence of selected MJUO and MSSSO spectra of RU Cen is displayed in Fig. 8. The metallic lines are extremely weak at all phases, while the carbon-enhanced nature of this star is confirmed by the presence of the C I line at 6587.622 Å. The Hα line is very strong at all phases but particularly strong just after primary minimum at phase ~ 0.1. Fig. 9 shows that the strongest emission is associated with the primary shock wave which is propagating through the line formation region at around phase 0.1, while a weaker Hα enhancement, associated with the secondary shock, is seen at phase 0.6.

Radial velocities were measured from the weak C I line at 6587.622 Å (see Table A3). Although some of the velocity measurements may be affected by noise due to the extreme weakness of the C I line, the radial velocity curve does show two velocity cycles during each 64.60-d luminosity cycle.

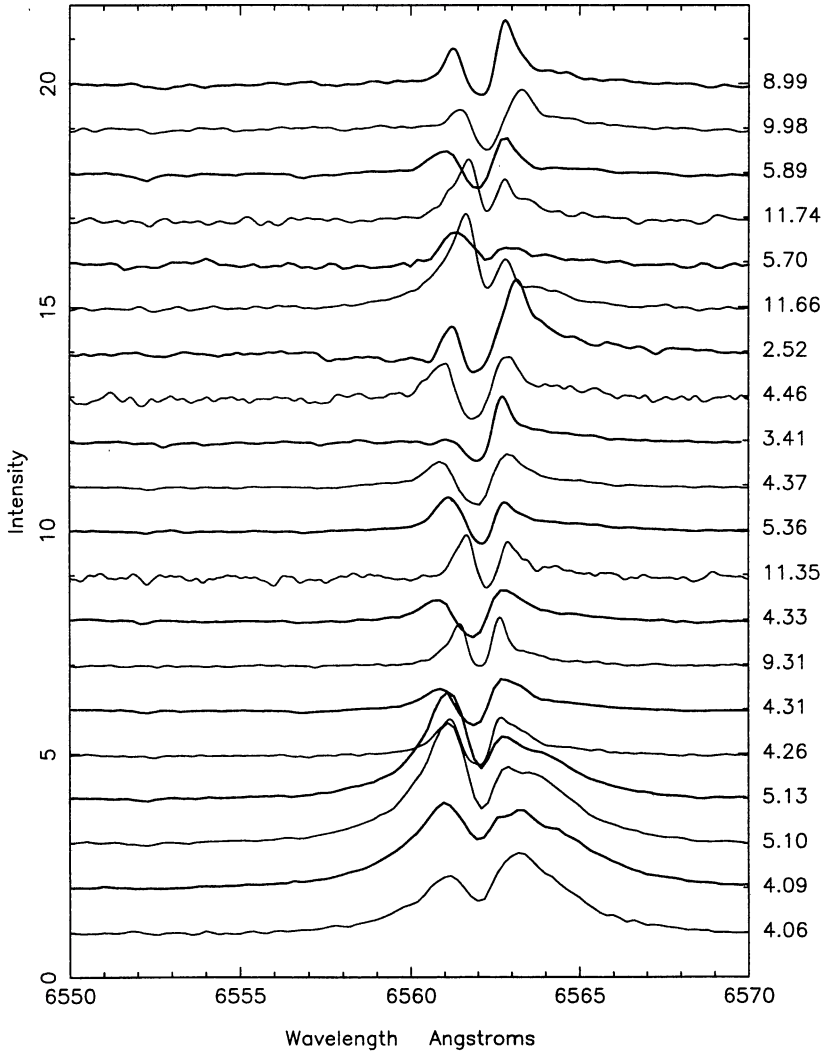


Figure 8. A selection of stacked MJUO and MSSSO spectra of the Hα region in RU Cen. The cycle number and phase are indicated to the right of each spectrum.

© Royal Astronomical Society • Provided by the NASA Astrophysics Data System

1997MNRAS.286....1P

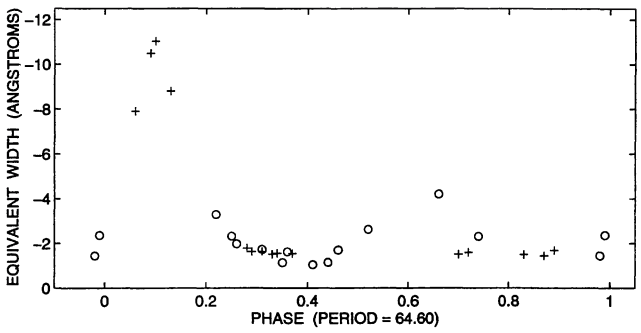


Figure 9. The phase dependence of the the Hα equivalent width in RU Cen. Equivalent widths were measured on both the MJUO (∘) and MSSSO (+) spectra.

3.4 AD Aql

The stacked spectra (Fig. 10) of AD Aql reveal that this star, like the other Preston type B object RU Cen, has very few metallic lines visible in its spectrum. The Hα profile shows a strong redward emission peak. Broad, shallow absorption wings are also present. Details of the spectroscopic observations are presented in Table A4.

The phase dependence of the Hα equivalent width is shown in Fig. 11. Strong Hα emission associated with the secondary shock wave is seen at phase 0.6. Hα emission associated with the primary shock wave is also indicated at about phase 0.1, but poor phase coverage around the primary minimum does not allow us to conclude whether the emission is stronger for the primary or the secondary shock. Profile fitting to the Hα line shows that the absorption component has a double-peaked radial velocity distribution indicative of two shocks per cycle (see Table A4).

3.5 V453 Oph

The two MSSSO spectra show that V453 Oph has few metallic lines, consistent with its spectroscopic classification as a Preston type C star and Cardelli's (1989) report of a metallicity of [Fe/H] = −1.6. Both MSSSO spectra obtained show double-peaked Hα emission and broad absorption wings. At phase 1.41 the Hα emission is about 1.1 times the continuum level while at phase

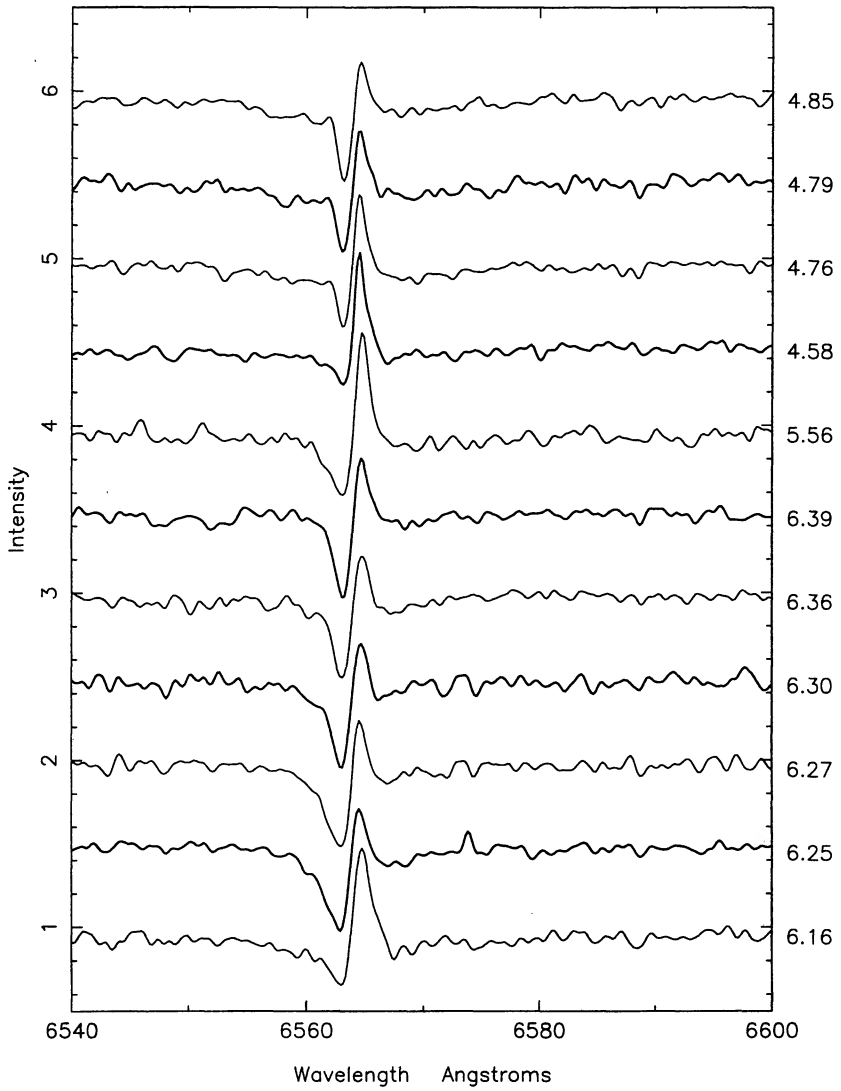


Figure 10. Stacked MSSSO spectra of the region around the Hα line in AD Aql. The phase and cycle number are indicated to the right of each spectrum.

© Royal Astronomical Society • Provided by the NASA Astrophysics Data System

1997MNRAS.286....1P

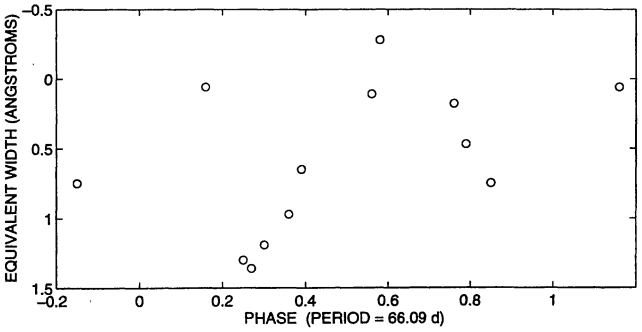


Figure 11. The phase dependence of the the Hα equivalent width in AD Aql.

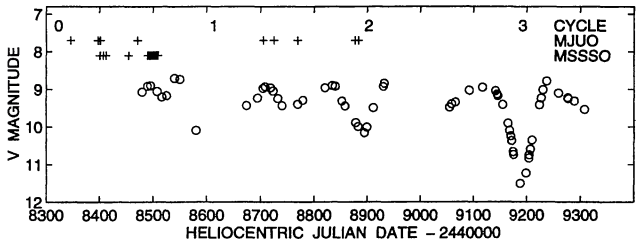


Figure 12. The light curve and spectral phase coverage for RY Ara. The MJUO photometric observations (∘) and the times of spectroscopic observations at both MJUO and MSSSO (+) are shown versus heliocentric Julian date. The beginning of each new cycle (according to the photometric ephemeris) is also indicated.

0.76 it is much greater, at ~ 1.8 times the level of the continuum. This stronger Hα emission occurs at the phase expected for emission associated with the secondary shock wave.

The radial velocities of the absorption and emission components of the Hα line for the two spectra are about $-120\,\mathrm{km\,s^{-1}}$ (see Table A5). A strong spectral feature at about 6613.4 Å has been tentatively identified as a diffuse interstellar band (Lloyd Evans, private communication). Using Herbig's (1975) relation between the equivalent width of this line and the stellar $E(B-V)$, we derive a mean $E(B-V)$ of 0.53 which is in good agreement with Cardelli's (1989) value of 0.50 derived from spectrophotometric observations. The velocities and other spectroscopic information are given in Table A5.

3.6 RY Ara

The MJUO *V* photometry and the dates when spectra were obtained of RY Ara at MJUO and MSSSO are shown in Fig. 12. Due to the lack of photometry before HJD ~ 244 8480, the photometric behaviour and consequently the photometric phases during cycle 0 are uncertain. Dates, phases and radial velocities are tabulated in Table A6.

Stacked spectra (Fig. 13) show that there is good phase coverage between 0.1 and 0.7 but only one spectrum between 0.7 and 0.1. The Hα profile is double-peaked at many phases with more emission seen on the blueward wing. Enhanced Hα emission is seen just after secondary light minimum at about phase 0.55. One spectrum was obtained at a phase of 0.11 when strong emission associated with the primary shock wave would be expected. However, this spectrum shows very little emission. Owing to the lack of contemporaneous photometry, we are unable to link this lack of emission with any peculiar photometric behaviour.

Like R Sct and other Preston type A stars, RY Ara displays numerous, relatively strong metallic lines at all phases. Emission or line doubling affects the Fe I line at 6546.245 Å during phases 0.28–0.35 and 0.54–0.57. It is possible that, due to the lower resolution of the MSSSO spectra, the line doubling may not be resolved, with the doubled Fe I line appearing as a blended line with a mean velocity. In addition, during phases 0.11–0.33 and 0.60–64 the Ti II line at 6554.238 Å displays shock-related emission behaviour. The radial velocity curve derived from the 6546.245-Å line of Fe I (Fig. 14) is consistent with two velocity cycles being present per 289.6-d photometric period.

The MSSSO spectrum taken at phase 0.48 displays very strong molecular absorption features. Molecular bandheads of the γ system of TiO are apparent at the wavelengths of 6651.5 and 6681.1 Å. Also evident in the MSSSO spectrum at this phase is the CN bandhead at 6631.3 Å. CN bandheads at 6383.906 and 6747.620 Å are visible on the MJUO spectra taken during phases 0.54–0.57 and 0.94, that is, around primary and secondary light minima.

3.7 V820 Cen

Owing to the very irregular nature of the light variations in V820 Cen, the period and therefore the calculated photometric phases are not very reliable. Fig. 15 shows a selection of MJUO and MSSSO spectra in phase sequence. The very weak metallic lines confirm the low-metallicity and high-velocity nature of V820 Cen, as reported by Wegner (1976) and Hunger & Kaufmann (1976).

A range of Hα profiles are seen. Large variations in the strength and broadness of the central absorption core, as well as changes in the overall strength of the emission, are apparent. The variation of the equivalent width of the Hα line was investigated. The times at which the Hα emission occurs in V820 Cen are different from those in the previously presented stars. Strong emission appears to occur during the descending branch of the light curve rather than the ascending branch as for the other, more convincing RV Tauri stars discussed in this paper. Combined with the irregularity of the light and colour variations (Pollard et al. 1996a), this is further evidence that V820 Cen may not be an RV Tauri star, but is more likely to be a semiregular variable.

Radial velocities of the Fe I line at 6546.245 Å were measured and these are presented in Table A7. The radial velocities and the light variations do appear to be correlated, with less negative radial velocities being associated with brighter *V* magnitudes.

3.8 U Mon

Fig. 16 shows the MJUO *V* light curve and indicates the dates when spectra of U Mon were obtained at MJUO and MSSSO. The spectra obtained at MJUO are shown in phase sequence in Fig. 17. Numerous lines of atomic species are apparent and these lines get particularly strong during phases 0.80–0.10. Molecular lines, mostly due to TiO with bandheads at 6159.1, 6214.9 and 6714.4 Å, are quite obvious in the spectra during these cool phases. The CN bandheads at 6383.906 and 6747.620 Å, which were seen in R Sct at both primary and secondary minimum, are also seen in U Mon at the same phases.

The phase dependence of the Hα equivalent width is presented in Fig. 18. It is quite apparent that during cycles 3–6 the Hα emission is much more intense than during cycles 9–14. As well as Hα emission associated with the two shock waves per luminosity cycle, it appears that there is a further contribution to, or enhancement of,

© Royal Astronomical Society • Provided by the NASA Astrophysics Data System

1997MNRAS.286....1P

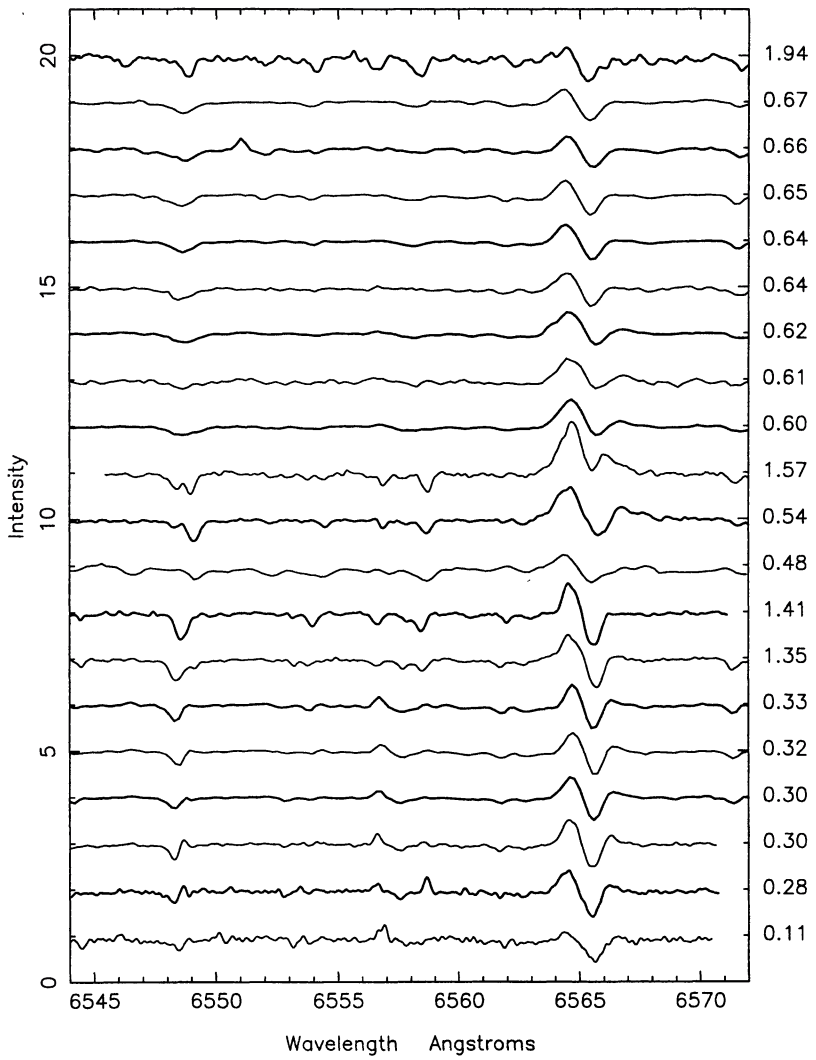


Figure 13. Stacked MSSSO and MJUO spectra of the region around the Hα line in RY Ara. The cycle number and phase are indicated to the right of each spectrum.

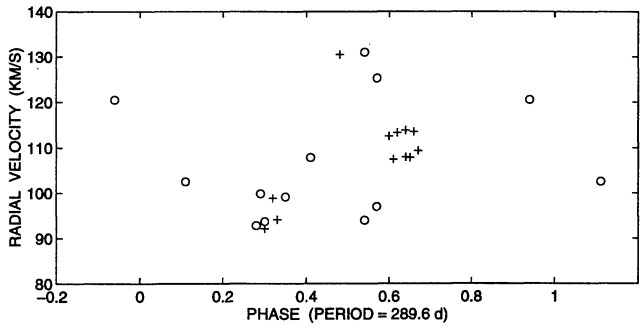


Figure 14. The radial velocities for RY Ara, measured from the Fe I line at 6546.245 Å using both MJUO (∘) and MSSSO (+) spectra. The phases are calculated using a period of 289.6 d.

the Hα emission during cycles 3–6. It is likely that the Hα enhancement is related to the long-term period in this RVb type star, since cycles 3–6 correspond to the minimum of the long-term period in U Mon (Pollard & Cottrell 1995).

During phases 0.2–0.3, most Fe I lines with excitation potentials between 2.0 and 3.0 eV display two components. Comparison of the U Mon spectra with those of R Sct reveals that the doubled components have a larger velocity spacing, indicating a greater intensity of the atmospheric shock wave. There are a variety of lines that display emission components. During phases 0.20–0.30 and 0.40–0.70, emission behaviour is strong in a number of Ti I lines.

Radial velocities were obtained (Fig. 19 and Table A8) using Fe I lines at 6200.321 and 6750.164 Å on the MJUO spectra and using the Fe I lines at 6546.245 Å on the MSSSO spectra. These lines appeared unblended and of sufficient strength to determine the radial velocities at all the observed phases. (The Fe I line at 6546.245 Å was not used to measure velocities on the MJUO spectra since emission components were present at some phases.) Two discontinuities are seen at phases ~ 0.2 and ~ 0.6 in the radial velocity curve phased using the 92.32-d period.

A large scatter is seen in the radial velocity curves which is in part due to the long-period radial velocity variations that have been reported for this star and other RV Tauri stars of the RVb subclass. The most likely explanation of these long-period radial velocity variations is orbital motion in a binary system (Pollard & Cottrell, in preparation).

3.9 AI Sco

The MJUO *V* photometry and the dates when spectra were obtained at both MJUO and MSSSO are shown in Fig. 20. All the spectra

© Royal Astronomical Society • Provided by the NASA Astrophysics Data System

1997MNRAS.286....1P

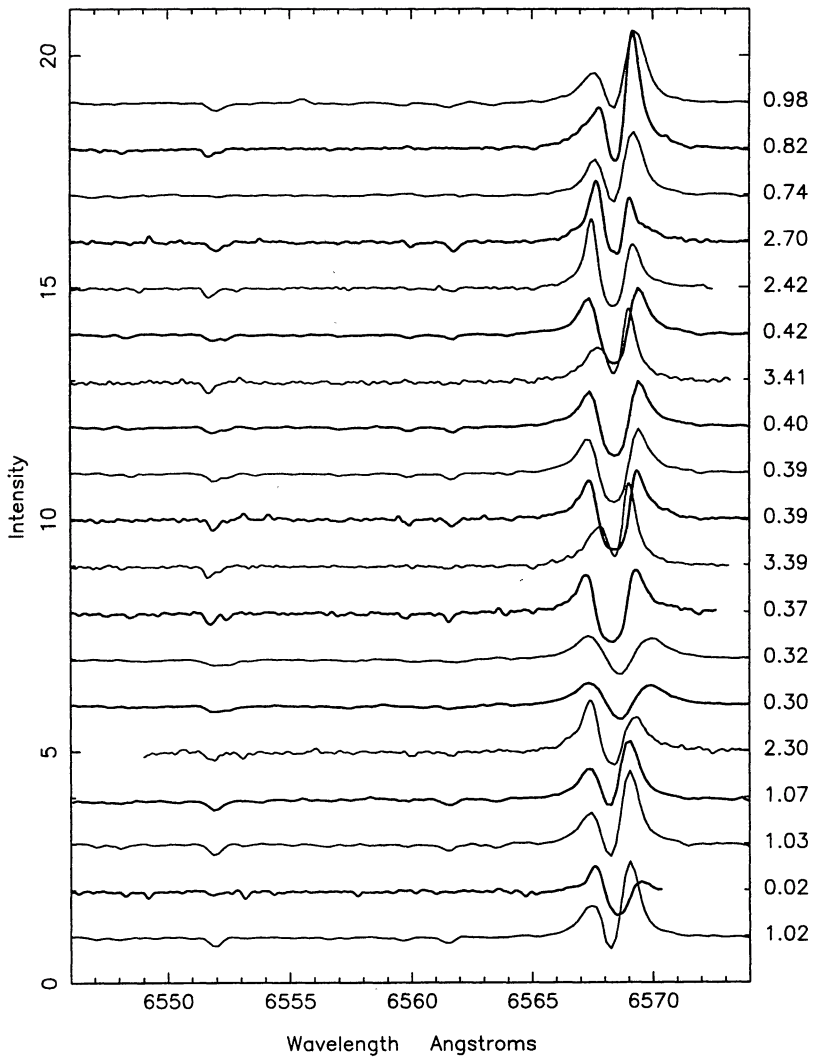


Figure 15. A selection of stacked MJUO and MSSSO spectra of V820 Cen. The cycle number and phase are indicated to the right of each spectrum.

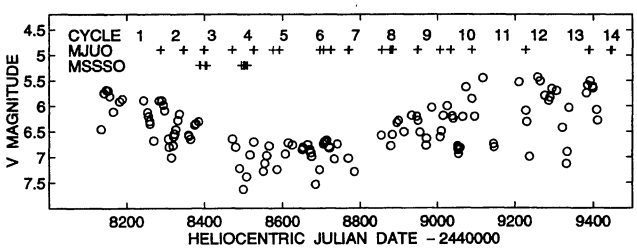


Figure 16. The light curve and spectral phase coverage for U Mon. The MJUO photometric observations (∘) and the times that spectroscopic observations were obtained at both MJUO and MSSSO (+) are shown versus heliocentric Julian date. The beginning of each new cycle (according to the photometric ephemeris) is also indicated.

were obtained while AI Sco was at the maximum of its long-period light variation.

The spectra are shown in phase sequence in Fig. 21. These spectra confirm the strong-lined nature of this star and reveal similarities to R Sct and U Mon, which are also Preston type A stars. For half the cycle the Hα profile shows strong extended blue absorption, perhaps indicative of mass outflow. Certainly the Hα radial velocities of up to 360 km s^{-1} are far in excess of the escape velocity of the star. A dramatic change in the appearance of the profile is apparent near phase 0.6. However, due to the small number of spectra obtained it is difficult to ascertain whether these changes are phase-dependent or whether they occur over a longer time-scale.

Radial velocities for the Fe I lines at 6546.245 and 6569.224 Å are plotted in Fig. 22 and tabulated in Table A9. The peak-to-peak amplitude is about 50 km s^{-1}, which is one of the largest amplitudes obtained for the programme RV Tauri stars. A discontinuity is apparent at phase ~ 0.64. This corresponds to the phase at which the metallic lines are extremely weak. The radial velocity curve is consistent with two velocity cycles being present per 70.03-d luminosity period.

3.10 AR Pup

The MJUO *V* photometry and the dates when spectra were obtained at both MJUO and MSSSO are shown in Fig. 23. The descending branch and the minimum of the long-period light variation have been sampled by the spectroscopic observations.

The most striking feature in the spectra is the strong emission line of Hα (Fig. 24). The Hα profile on the MJUO spectra appears to be

© Royal Astronomical Society • Provided by the NASA Astrophysics Data System

1997MNRAS.286....1P

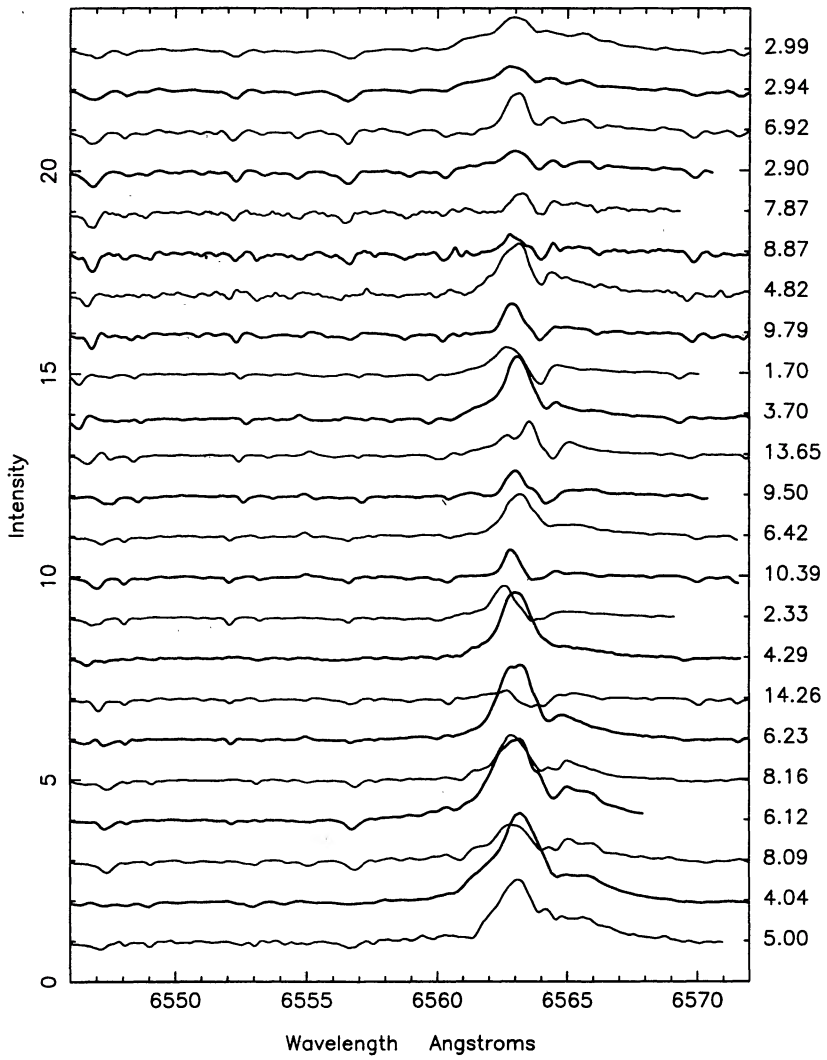


Figure 17. A selection of spectra of the region around Hα in U Mon. The cycle number and phase of observation are indicated at the right of each spectrum.

quite simple with no obvious multiple components, except for the spectrum obtained at phase 0.97. From the more extensive wavelength coverage of the MSSSO spectra, shallow (< 10 per cent), broad ($\Delta\lambda \sim 40$ Å) Hα absorption is apparent.

The phase dependence of the Hα emission strength is shown in Fig. 25 and is also included in Table A10. The periodic nature of the strength of the Hα equivalent width is quite apparent with peaks in the Hα line strength occurring at phases ~ 0.15 and ~ 0.65. This is similar behaviour to what is observed to occur in the other RV Tauri stars and provides evidence for the presence of two shock waves per luminosity period. Cycle-to-cycle variations in the emission strength are seen between phases 0.0 and 0.2.

Very few metallic lines are seen in AR Pup. An extremely weak line of C I (6587.622 Å) is visible on the MSSSO spectra and the radial velocities of this line are shown in Table A10.

3.11 IW Car

The spectra are shown in phase sequence in Fig. 26. As shown in Fig. 27(a), the light variations in IW Car are quite irregular and, even though the spectroscopic sampling is reasonably extensive, the phasing of these spectra is very imprecise.

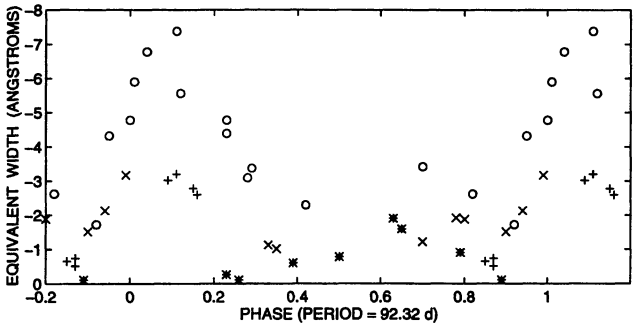


Figure 18. The Hα equivalent width of U Mon plotted versus phase with different symbols used to differentiate between the different cycles. The symbols are as follows: cycles 1–2 (×), cycles 3–6 (∘), cycles 7–8 (+) and cycles 9–14 (∗).

The spectra (Fig. 26) reveal very few metallic lines, which is consistent with the low metallicity ([Fe/H]~ − 1.0) reported by Giridhar, Kameswara Rao & Lambert (1994). No shock-related spectral features, apart from Hα emission wings, are seen. It is therefore possible that IW Car is not an RV Tauri star and the Hα emission arises from mass loss to a circumstellar shell or mass transfer in the binary system.

© Royal Astronomical Society • Provided by the NASA Astrophysics Data System

1997MNRAS.286....1P

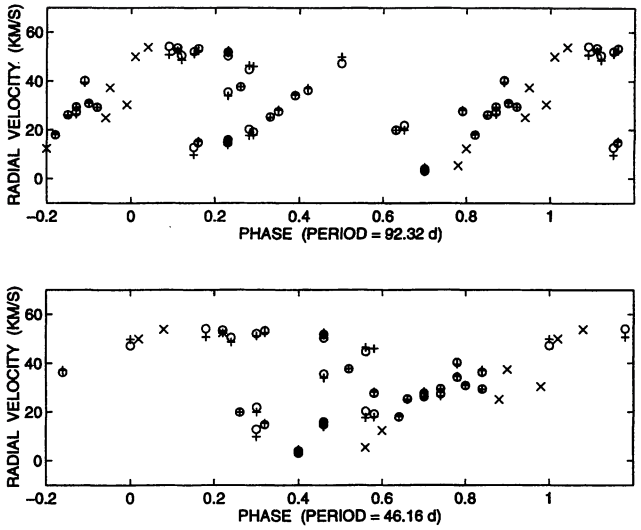


Figure 19. Radial velocity curves for U Mon. On the MJUO spectra the radial velocities were measured from the Fe I lines at 6200.321 Å (∘) and 6750.164 Å (+), while the Fe I line at 6546.245 Å (×) was used on the MSSSO spectra. Top panel = 'formal' period; bottom panel = 'fundamental' period.

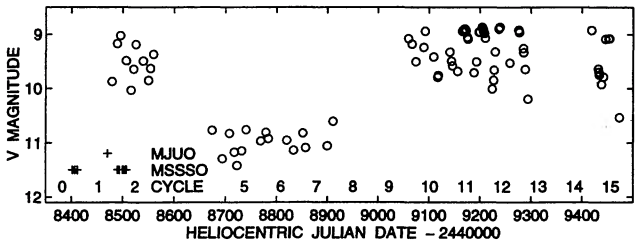


Figure 20. The light curve and spectral phase coverage for AI Sco. The MJUO photometric observations (∘) and the times when spectroscopic observations were obtained at both MJUO and MSSSO (+) are shown versus heliocentric Julian Date. The beginning of each new cycle (according to the photometric ephemeris) is also indicated.

The measurement of the Hα equivalent widths was complicated by the fact that broad ($\Delta\lambda\sim$ 30 Å), slightly blueshifted Hα absorption is present on all of the spectra. The MJUO spectra,with their short wavelength coverage, will have had the continuum placed too low and therefore the equivalent widths will be too small when compared with the MSSSO spectra. No dependence of the Hα equivalent width on the 72.0-d period was apparent.

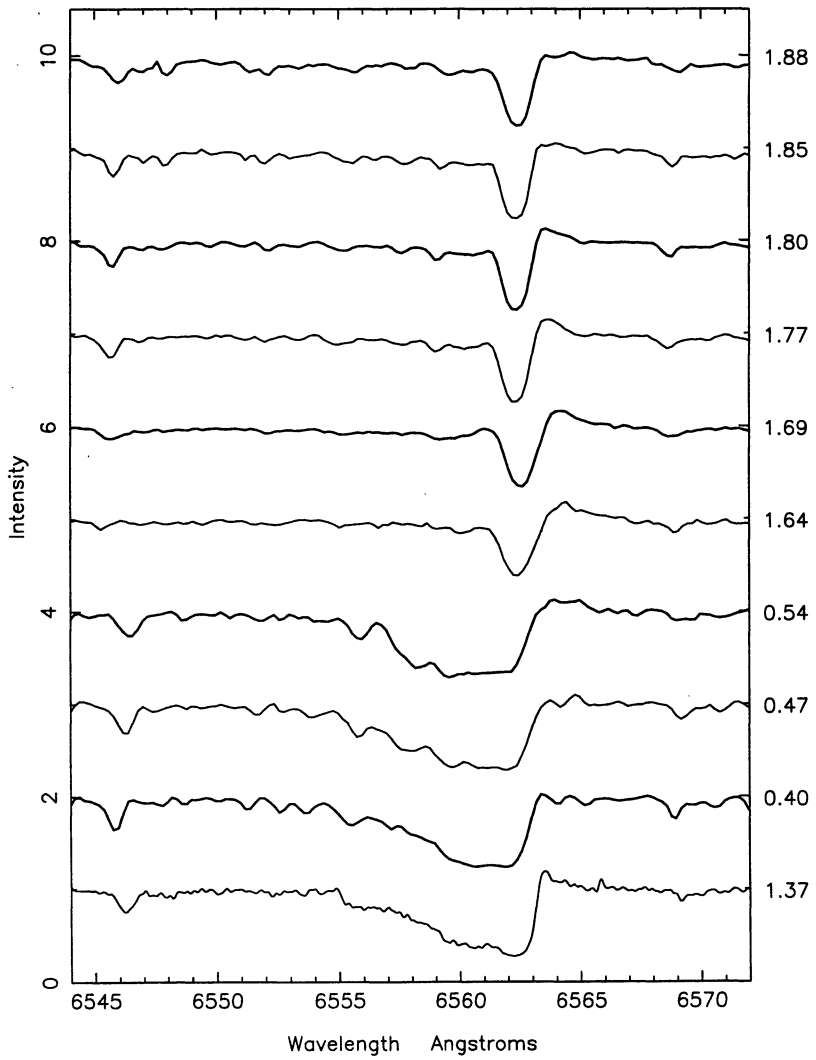


Figure 21. Stacked spectra of the Hα region in AI Sco. The cycle number and phase are indicated to the right of each spectrum.

© Royal Astronomical Society • Provided by the NASA Astrophysics Data System

1997MNRAS.286....1P

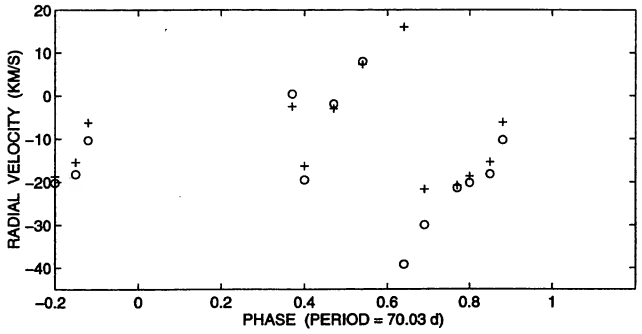


Figure 22. The radial velocities for AI Sco, measured from the Fe I lines at 6546.245 Å (∘) and at 6569.224 Å (+).

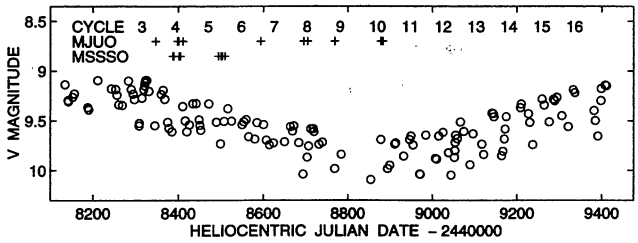


Figure 23. The light curve and spectral phase coverage for AR Pup. The MJUO photometric observations (∘) and the times when spectroscopic observations were obtained at both MJUO and MSSSO (+) are shown versus heliocentric Julian Date. The beginning of each new cycle (according to the photometric ephemeris) is also indicated.

Radial velocities were measured for the S I lines at 6743.575, 6748.779 and 6757.195 Å on the MJUO spectra and the 6587.622-Å C I line on the MSSSO spectra. Radial velocities were also measured from the narrow absorption component of the Hα line (see Table A11). Fig. 27 shows the Hα and metallic-line radial velocities from MJUO and MSSSO, as well as the contemporaneous photometric *V* photometry from MJUO.

The dominant trend seen in the Hα velocity curve is correlated with the long-term period in the light curve. The amplitude of the long-term radial velocity variations is estimated to be 35 km s^{-1}, although this is only a lower limit since it is uncertain whether both maximum and minimum of the long-term cycle have been sampled. The short-term phase dependence of the Hα velocities was investigated but no obvious trend with the 72.0-d photometric

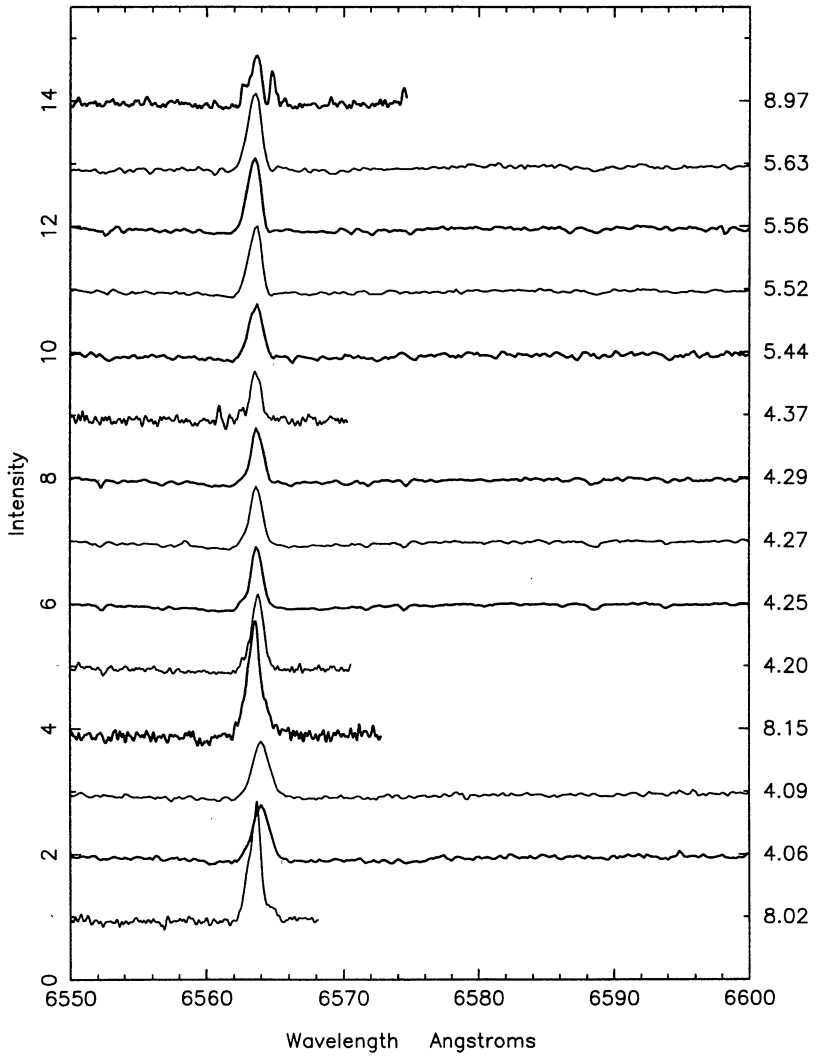


Figure 24. Selected MJUO and MSSSO spectra stacked in phase sequence. The region around the Hα line in AR Pup is shown. The cycle number and phase are indicated to the right of each spectrum.

© Royal Astronomical Society • Provided by the NASA Astrophysics Data System

1997MNRAS.286....1P

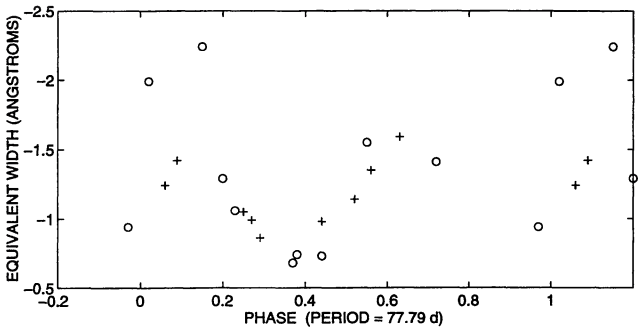


Figure 25. The phase dependence of the Hα equivalent width in AR Pup. Equivalent widths for the MJUO (∘) and MSSSO (+) spectra are plotted versus phase.

period was seen. Fig. 27(c) shows that there is both short- and long-term variability of the metallic radial velocities. The amplitudes of the long-term radial velocity variation are similar for the metallic lines and the Hα line.

IW Car has been reported to be a binary system. Houk (1978) gives a spectral classification of (A4 Ib–II: + F7/F8), noting that the A-type star has very sharp lines. However, from the derived MJUO radial velocities, we associate the narrow Hα absorption and emission features and the sharp absorption features in the spectra with the metal-poor F-type star. All of the spectral lines measured appear to be from a single star (giving the same radial velocity) except, perhaps, for the broad Hα absorption. It is possible that this feature arises from gas that is escaping from the star.

4 DISCUSSION

4.1 Hα emission profiles

Emission components for the Hα line were seen for every star in the RV Tauri programme. These emission components were present for most, if not all, of the pulsation cycle. In most stars the Hα profiles were consistent with increased emission following the passage of two shock waves through the stellar photospheres at around phases 0.1 and 0.6.

The most plausible explanation for the characteristic double- or multi-peaked emission profile of the Hα line is that it is the combination of an emission component and an absorption component that form in different layers of the atmosphere. Emission lines

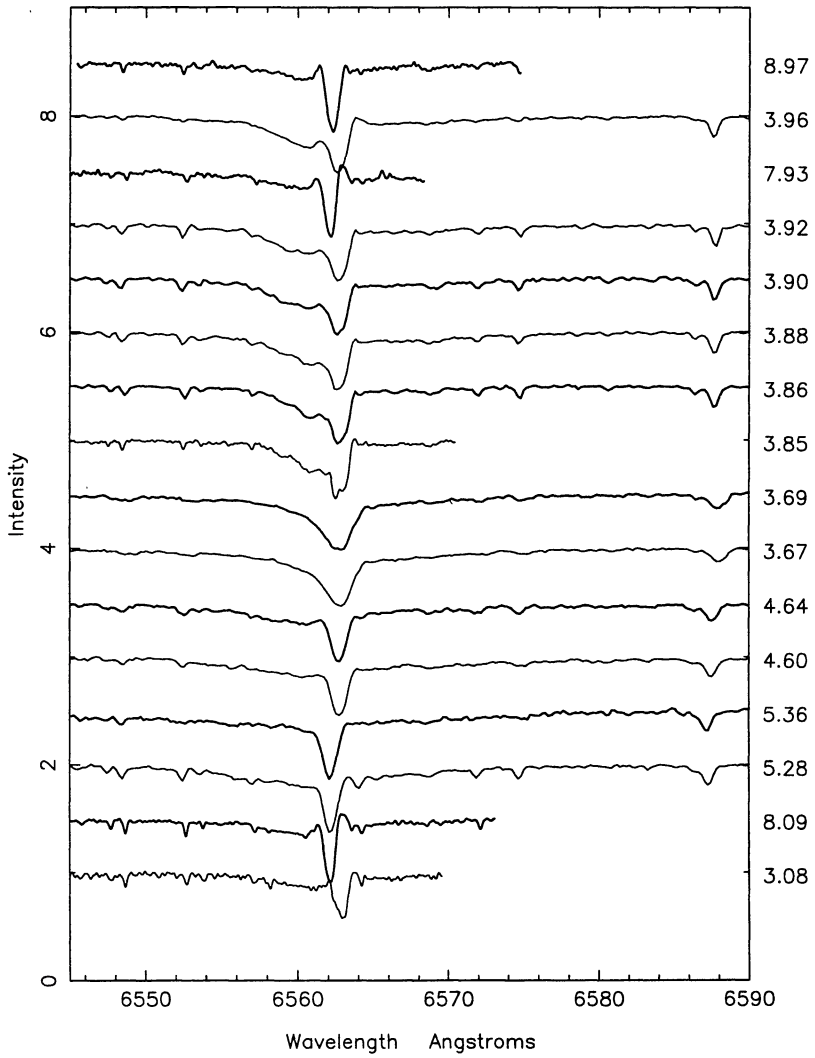


Figure 26. A selection of MJUO and MSSSO spectra of IW Car stacked in phase sequence. The cycle number and phase are indicated to the right of each spectrum.

© Royal Astronomical Society • Provided by the NASA Astrophysics Data System

1997MNRAS.286....1P

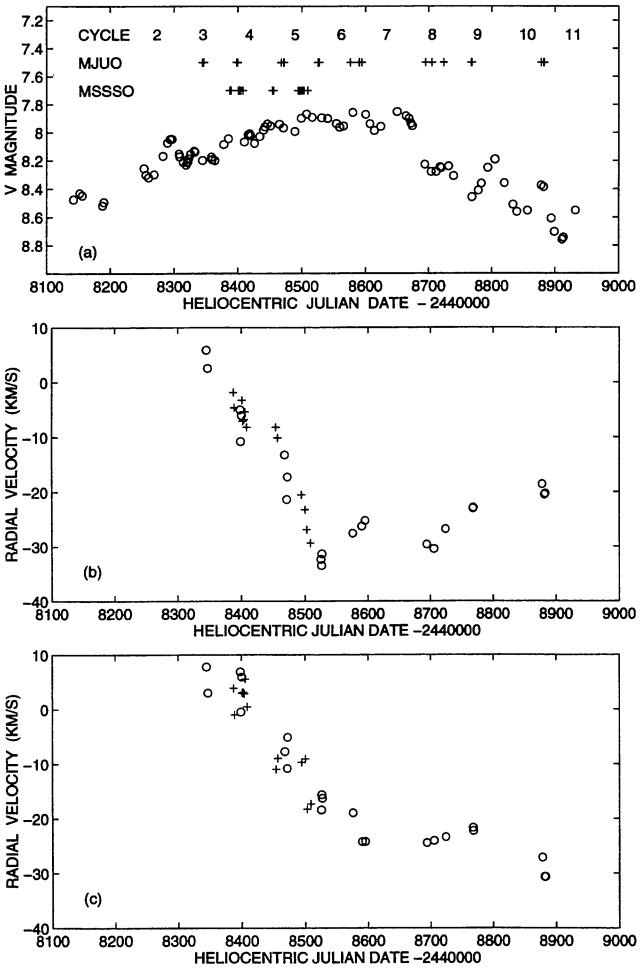


Figure 27. The light curve (a), Hα radial velocity curve (b) and metallic radial velocity curve (c) for IW Car. In (a), the MJUO photometry (∘), the times of spectra (+) and the cycle number are displayed. In (b), MJUO (∘) and MSSSO (+) Hα radial velocities are plotted. In (c), the radial velocities for the S I lines (∘) on MJUO spectra and C I lines (+) on MSSSO spectra are shown.

form within the de-excitation zone of the shock wave that propagates through the stellar atmosphere, and absorption lines are the result of either photospheric absorption or possibly Hα self-absorption above the shock front. The Hα line certainly forms over a very extended range of atmospheric layers and, because of this, an emission contribution to the Hα line from shock-heated gas is present for much of the pulsational cycle. This is in contrast to the metallic lines, which display emission components only when the shock wave is traversing the atmospheric layer where these lines are forming.

Large cycle-to-cycle variations in the appearance of the Hα profile have been noted. These variations may be indicative of differences in the shock intensity and the instantaneous state of the atmosphere, so that after one cycle the star does not return to exactly the same state. If during successive cycles shock waves possessing different intensities are produced, these can subsequently affect the relative extension of the stellar atmosphere and the propagation (and therefore the apparent phase) of the following shock wave. Wallerstein & Elgar (1992) use the analogy of waves breaking on a beach to investigate whether shock waves of differing amplitudes can explain the alternating behaviour of deep and shallow light minima in RV Tauri stars.

The Hα variability in the RVb-type members appears more complex than that of the RVa types. In U Mon and AR Pup, there appear to be two types or sources of variability. One contribution to the enhanced Hα emission arises from pulsational-phase-dependent emission associated with the shock waves, as discussed above. The second contribution to the emission is a longer-term effect, which, in U Mon, appears to be correlated with the long-term light, colour and radial velocity variations reported for this star (Pollard & Cottrell 1995). Both AI Sco and IW Car have strong, extended blue absorption which may be associated with mass outflow.

4.2 The metallic and molecular line behaviour

The metallic and molecular lines showed quite different behaviour from the Hα line, although consistency between lines of the same element and similar excitation potential was seen. The sequence of line profiles that was observed in the stars with good phase coverage (e.g. R Sct and U Mon) suggests that there is a phase lag between the upper and lower atmospheric layers, so that, when the lower atmosphere starts pulsating outwards, the higher layers are still infalling after the passage of a previous shock front.

The RV Tauri stars in this study display a metal-line radial velocity curve that is consistent with there being discontinuities at phases ~0.2 and ~0.6 so that the period is half that of the 'formal' or luminosity period. However, many stars did not have sufficient phase coverage to do more than suggest the form of the radial velocity curve. Cycle-to-cycle variations complicate the interpretation of these radial velocity curves and, in addition, the RVb stars are known to have long-period trends in their radial velocities. An additional ambiguity arises from the interpretation of the metallic-line profile when these are affected by the shock waves. A 'double' or 'split' line may be interpreted as two absorption components or, alternatively, as a narrow emission component superimposed on a broader absorption component. In all stars we have attempted to use metallic lines that are not strongly affected by the shock waves. Table 3 presents a summary of the radial velocity and light curve amplitudes.

The spectroscopic behaviour of V820 Cen is different from that of the other programme stars and this, together with its photometric irregularity, suggests that this star belongs to the related class of semiregular variables.

4.3 Pulsational models of RV Tauri stars

Although many different explanations of the alternation of deep and shallow minima in the light curves of the RV Tauri stars have been proposed (Takeuti & Petersen 1983; Aikawa & Bruegman 1987; Buchler & Kovács 1987; Fokin 1994), it is well established that the underlying variability arises from pulsations.

A fundamental question is whether the underlying period of the RV Tauri stars is the 'formal' period (defined as the time between two successive deep minima) or the so-called 'fundamental' period (the time between two successive minima). This study and previous optical spectroscopic studies have shown that the periodicity associated with the pulsational characteristics is half the formal period with two shock waves and two radial velocity cycles per formal period. However, infrared spectroscopic studies (Mozurkewich et al. 1987; Pollard et al. 1996c; Hinkle, Pollard & Wahlgren 1996) have found that the atomic absorptions in R Sct are always single-lined and trace out a continuous, repeatable pulsation of ~ 142 d which is equal to the 'formal' period.

It is possible that both optical and infrared studies can be

© Royal Astronomical Society • Provided by the NASA Astrophysics Data System

1997MNRAS.286....1P

Table 3. Summary of RV Tauri radial velocity and light curve amplitudes.

Star	Preston type	spectral line(s)	rad. vel. range ($km\,s^{-1}$)	Δ rad. vel.[a] ($km\,s^{-1}$)	ΔV (mag)	molecular bands
RVa photometric subclass						
R Sct	A	Fe I	+14.0 to +58.9	45	3.0	TiO, CN
AR Sgr	A	Hα	−103.1 to −87.9	~15	1.8	TiO, CN
RU Cen	B	C I	−63.9 to −47.8	~16	1.3	–
AD Aql	B	Hα	+32.7 to +72.1	~39	0.8	–
V453 Oph	C	Hα	−125.2 to −119.2	>6.0	1.0	–
RY Ara	A?	Fe I	+92.1 to +133.3	41	2.8	TiO, CN
V820 Cen	–	Fe I	−269.6 to −249.0	~21	0.8	–
RVb photometric subclass						
U Mon	A	Fe I	+2.0 to +53.2	>50	2.2	TiO, CN
AI Sco	A	Fe I	−39.2 to +8.0	>47	2.6	–
AR Pup	B	C I	+40.0 to +53.7	>14	1.0	–
IW Car	B	S I & C I	−30.6 to +7.8	>38	0.9	–

[a]The radial velocity amplitude is indicated where this is known precisely from measurements of line splitting; an approximate radial velocity amplitude is indicated when the phase coverage is poor and the amplitude is not well defined; a lower limit for the radial velocity amplitude (which also includes the long-term radial velocity variation) is given for the RVb-type stars.

consistent if we realize that we are probing different depths in the star at the different wavelengths. The 2-μm region appears to be an important region at which to observe these stars, since the H^- opacity is near its minimum and is five times less than at 5000 Å, enabling deeper layers to be investigated. Optical studies sample higher layers in the stellar atmosphere which are affected more by the shock waves.

A recent theoretical study by Fokin (1994) examines non-linear pulsations in RV Tauri star models. The high non-adiabaticity of the pulsation results in the pulsations having the form of a running wave, that is, non-synchronously moving layers, even in the interior mass zones. The model predicts that two shock waves are produced during each luminosity cycle. The primary shock has an amplitude of $< 40\,km\,s^{-1}$ which is in good agreement with the shock amplitudes measured for R Sct and AC Her (Gillet et al. 1990) and for the stars studied in this paper. A second, weaker ($\sim 20\,km\,s^{-1}$) shock is generated near the photosphere just before the secondary light minimum. This model is consistent with the fact that the infrared observations show a period that is equal to the time between successive deep minima, since the first overtone is not important in the deeper layers and shock generation occurs above the layers that are being sampled by the infrared spectroscopy. The optical studies, however, sample the region where the two shock waves are produced and the first overtone is an important factor.

5 CONCLUSIONS AND FUTURE WORK

In this paper we have presented the results of a long-term, high-resolution spectroscopic study of eleven RV Tauri stars. Stars from all three Preston spectroscopic subtypes and both RVa and RVb photometric subtypes were included. All stars in the programme displayed an emission contribution to the Hα profile. Enhanced Hα emission, consistent with the passage of two shock waves through the stellar photospheres, was observed at around phases 0.1 and 0.6.

At these phases, discontinuities in the Fe I radial velocity curves were also apparent in the Preston type A stars. The more metal-deficient nature of the Preston type B and C stars was obvious with these stars having a more 'veiled' appearance. Preston type B stars are carbon-enhanced and radial velocities were generally measured from the higher excitation potential C I line at 6587.622 Å. The Preston type C object,V453 Oph, displayed a strong line at about 6613.4 Å which we have tentatively identified as a diffuse interstellar band. Most of the RV Tauri radial velocity curves showed, or were consistent with, two radial velocity cycles per photometric period. All members of the Preston A spectroscopic subtype (except AI Sco) showed molecular bands of TiO and CN at minimum light, whereas the B and C types did not show any strong molecular bands.

Further spectroscopic observations are required to address a number of outstanding issues concerning the nature of the RV Tauri stars.

(1) Lines of different excitation potential can be used as probes of different depths in the stellar photosphere, allowing stratification effects to be investigated. The lower excitation potential lines, such as those of Ti I, tend to form higher in the atmosphere and show strong shock-related emission features. The deeper-forming lines of higher excitation potential are more likely to track the underlying pulsation. Infrared spectroscopy would be most useful in this respect.

(2) High-resolution spectroscopy through several pulsation cycles at long-term light minimum and at long-term light maximum of a number of RVb stars would be useful in establishing whether there are any changes in the stellar temperature, the spectroscopic class, and the appearance and amplitude of the radial velocity curve during the long-term minimum.

(3) An abundance analysis of a reasonable sample of the RV Tauri stars would be useful for a more quantitative assessment of the relationship between the members of the three spectroscopic subtypes. A knowledge of the physical properties of individual stars is an important step towards a better understanding of their evolutionary status. The difficulties at this stage arise from the tremendously dynamic nature of the photospheres of these stars. Complications that must be considered are the presence of strong atmospheric shocks, the subsequent huge extension of the atmosphere and the complex emission behaviour of many photospheric lines.

ACKNOWLEDGMENTS

This work is based on part of KRP's PhD thesis at the University of Canterbury. We would like to thank the former director of MSSSO, Dr Alex Rodgers, for the generous allocation of telescope time on

© Royal Astronomical Society • Provided by the NASA Astrophysics Data System

1997MNRAS.286....1P

the 1.9-m telescope at MSSSO in 1991. We are grateful to Professor John Percy and Dr Tom Lloyd Evans for their useful comments and suggestions on an earlier version of this paper. During the course of this research, financial support for KRP was gratefully received from: the New Zealand University Grants Committee; the Ministry of Research, Science and Technology; Zonta International; the Department of Physics and Astronomy, University of Canterbury; the Royal Society of New Zealand and the Kingdon–Tomlinson Bequest administered by the The Royal Astronomical Society of New Zealand.

REFERENCES

Aikawa T., Bruegman O., 1987, Ap&SS, 137, 115
Albrow M. D., 1994, PhD thesis, University of Canterbury
Buchler J. R., Kovács G., 1987, ApJ, 320, L57
Cardelli J. A., 1989, AJ, 98, 324
Fokin A. B., 1994, A&A, 292, 133
Gillet D., Duquennoy A., Bouchet P., Gouiffes C., 1989, A&A, 215, 316
Gillet D., Burki G., Duquennoy A., 1990, A&A, 237, 159
Giridhar S., Kameswara Rao N., Lambert D. L., 1994, ApJ, 437, 476
Herbig G. H., 1975, ApJ, 196, 129
Hinkle K. H., Pollard K. R., Wahlgren G. M., 1996, in Morrison H., Sarajedini A., eds, ASP Conf. Ser. Vol. 92, Formation of the Galactic Halo...Inside and Out. Astron. Soc. Pac., San Francisco, p. 204
Houk N., 1978, Michigan Spectral Catalogue of Two-dimensional Spectral Types for the HD Stars, Vol. 1. University of Michigan, Ann Arbor
Hunger K., Kaufmann J. P., 1976, A&A, 50, 133
Joy A. H., 1950, PASP, 62, 60
Joy A. H., 1952, ApJ, 115, 25
Kholopov P. N., Samus N. N., Durlevich O. V., Kazarovets E. V., Kireeva N. N., Tsvetkova T. M., 1985, General Catalogue of Variable Stars, 4th edn. Nauka Publishing House, Moscow
Lawson W. A., Kilkenny D., Marang F., van Wyk F., Pollard K. R., Ryder S. D., 1993, MNRAS, 265, 351
Lèbre A., Gillet D., 1991a, A&A, 246, 490
Lèbre A., Gillet D., 1991b, A&A, 251, 549
Luck R. E., 1981, PASP, 93, 211
McLaughlin D. B., 1938, Publ. Obs. Univ. Michigan, 94, 94
Mozurkewich D., Gehrz R. D., Hinkle K. H., Lambert D. L., 1987, ApJ, 314, 242
Payne-Gaposchkin C., Brenton V. K., Gaposchkin S., 1943, Harv. Ann., 113, 1
Pollard K. R., Cottrell P. L., 1995, in Stobie R. S., Whitelock P. A., eds, Proc. IAU Colloq. 155, ASP Conf. Ser. Vol. 83. Astrophysical Applications of Stellar Pulsation. Astron. Soc. Pac., San Francisco, p. 409
Pollard K. R., Cottrell P. L., Kilmartin P. M., Gilmore A. C., 1996a, MNRAS, 279, 949
Pollard K. R. et al., 1996b, in Ferlet R., Maillard J.-P., eds, Proc. 12th IAP Colloq., Variable Stars and the Astrophysical Returns of Microlensing Surveys, in press
Pollard K. R., Hinkle K. H., Cottrell P. L., Lawson W. A., Wahlgren G. M., 1996c, in Pallavicini R., Dupree A. K., eds, Proc. 9th Cambridge Workshop, ASP Conf. Series, in press
Preston G. W., 1962, ApJ, 136, 866
Preston G. W., 1964, ApJ, 140, 173
Preston G. W., Krzeminski W., Smak J., Williams J. A., 1963, ApJ, 137, 401
Rosino L., 1951, ApJ, 113, 60
Takeuti M., Petersen J. O., 1983, A&A, 117, 352
Wallerstein G., Cox A. N., 1984, PASP, 96, 677
Wallerstein G., Elgar S., 1992, Sci, 256, 1531
Wallerstein G., Jacobsen T. S., Cottrell P. L., Clark M., Albrow M. D., 1992, MNRAS, 259, 474
Wegner G., 1976, Observatory, 96, 13

APPENDIX A: SPECTRA OF THE RV TAURI STARS

This appendix contains the tabulated spectroscopic data for the programme RV Tauri stars. The data are generally arranged in columns as follows: the heliocentric Julian date −244 0000 for the mid-time of observation, the spectroscopic region (if regions other than Hα were observed), the observing site (1=MJUO, 2=MSSSO), the photometric phase, the Hα equivalent width and metal line (or, in some cases, the Hα line) radial velocity for each observation. The tables are numbered in the order that they are discussed in Section 3 of this paper.

Table A1. Spectroscopic observations of R Sct.

HJD	region	site	phase	W_λ	Fe I radial velocities		
					6546.245 Å	6569.224 Å	6750.164 Å
2440000+			(ϕ)	(Å)	(km s^{-1})	(km s^{-1})	(km s^{-1})
8342.238	Hα	1	2.00	−0.15	51.4	–	51.6
8347.203	Hα	1	2.03	−0.04	51.8	–	52.7
8387.180	Hα	2	2.24	−0.07	19.2, 56.1	27.0	–
8389.199	Hα	2	2.25	−0.06	21.5, 55.3	28.8	–
8397.086	Hα	1	2.31	+0.10	30.3	30.7	30.5
8398.164	Hα	1	2.32	+0.18	31.8	32.3	33.1
8398.199	Na	1	2.32	–	–	–	–
8399.141	Hα	1	2.32	+0.21	31.8	32.2	32.8
8400.070	Hα	1	2.33	+0.18	31.8	–	32.0
8401.137	Hα	2	2.34	+0.36	30.3	30.4	–
8401.141	Hα	1	2.34	+0.26	30.8	31.6	32.1
8403.102	Hα	2	2.35	+0.45	29.2	37.3	–
8407.211	Hα	2	2.38	+0.44	36.4	37.8	–
8408.086	Hα	2	2.39	+0.40	39.8	40.3	–
8412.125	Hα	2	2.42	+0.38	41.3	41.5	–
8414.109	Hα	1	2.43	+0.44	39.8	40.4	40.1
8453.105	Hα	2	2.71	−0.38	38.2	32.8	–
8455.145	Hα	2	2.72	−0.18	38.1	33.6	–
8466.945	Hα	1	2.81	+0.26	30.8	31.6	31.4
8467.906	Hα	1	2.81	+0.27	32.2	33.4	32.7
8470.969	Hα	1	2.84	+0.40	34.8	36.0	35.6
8471.961	Hα	1	2.84	+0.42	35.4	36.7	36.4
8489.945	Hα	2	2.97	+0.83	50.0	52.5	–

© Royal Astronomical Society • Provided by the NASA Astrophysics Data System

1997MNRAS.286....1P

Table A1 – *continued*

HJD	region	site	phase	W_λ	Fe I radial velocities		
					6546.245 Å	6569.224 Å	6750.164 Å
2440000+			(ϕ)	(Å)	(km s^{-1})	(km s^{-1})	(km s^{-1})
8492.996	Hα	2	2.99	+0.77	53.4	55.1	–
8495.043	Hα	2	3.01	+0.65	52.0	54.2	–
8500.023	Hα	2	3.04	−0.02	52.8	52.0	–
8502.043	Hα	2	3.05	−0.32	18.6, 50.2	58.0	–
8503.059	Hα	2	3.07	−0.41	16.8, 49.0	59.2	–
8505.035	Hα	2	3.08	−0.53	14.0, 49.6	59.1	–
8507.012	Hα	2	3.09	−0.79	19.0, 58.2	22.0	–
8509.063	Hα	2	3.11	−0.76	16.6, 58.9	21.0	–
8512.055	Hα	2	3.13	−0.42	18.6, 58.3	20.5	–
8524.871	Hα	1	3.22	+0.54	23.3	25.8	24.5
8525.914	Hα	1	3.23	+0.54	23.7	27.0	25.4
8525.949	Na	1	3.23	–	–	–	–
8526.957	Hα	1	3.24	+0.58	24.8	28.1	26.5
8706.242	Hα	1	4.51	+0.92	51.1	48.6	50.2
8724.164	Hα	1	4.64	+0.28	27.3, 52.9	30.5	29.7, 53.8
8768.031	Hα	1	4.92	+0.82	44.0	40.9	40.4
8768.164	Na	1	4.92	–	–	–	–
8876.855	Hα	1	5.73	+0.00	22.2	24.1	23.1
8877.063	Na	1	5.73	–	–	–	–
8878.004	Hα	1	5.74	+0.13	23.4	25.4	23.7
8880.914	Hα	1	5.76	+0.29	24.8	27.2	25.9
8882.902	Hα	1	5.77	+0.37	26.2	28.4	26.5
9089.238	Hα	1	7.22	−0.41	28.7, 55.5	28.9	29.5, 56.4
9115.168	Hα	1	7.43	+0.46	51.2	52.1	50.5
9117.156	Hα	1	7.44	+0.53	52.6	53.6	53.1
9118.188	Hα	1	7.45	+0.51	52.8	53.8	53.1
9224.938	Hα	1	8.21	−0.10	56.0	–	58.3

Table A2. Spectroscopic observations of AR Sgr.

HJD	site	phase	W_λ	radial velocity	
				Hα ab	Hα em
2440000+		(ϕ)	(Å)	(km s^{-1})	(km s^{-1})
8402.082	2	0.45	−1.39	−106.0	−111.2
8412.121	2	0.56	−1.96	−100.3	−102.5
8414.188	1	0.58	−2.96	−103.1	−101.4
8454.086	2	1.03	−2.77	−90.7	−90.7
8471.137	1	1.22	−2.00	−93.9	−96.9
8490.965	2	1.45	−0.16	−93.8	−99.2
8500.094	2	1.55	−0.79	−107.3	−107.3
8501.127	2	1.56	−1.28	−87.9	−96.0
8503.086	2	1.58	−1.62	−103.1	−103.6
8505.137	2	1.60	−1.46	−101.4	−105.7
8507.117	2	1.63	−1.53	−98.4	−101.8
8509.129	2	1.65	−1.60	−107.7	−107.3
8512.082	2	1.68	−0.88	−106.6	−107.2
8769.246	1	4.58	−1.74	−103.4	−101.0
8881.938	1	5.85	−1.59	−107.4	−103.5

Table A3. Spectroscopic observations of RU Cen.

HJD	site	phase	W_λ	C I rad. vel. 6587.622 Å
2440000+		(ϕ)	(Å)	(km s^{-1})
8287.125	1	2.52	−2.62	–
8345.125	1	3.42	−1.05	–
8346.984	1	3.44	−1.15	–
8386.910	2	4.06	−7.91	–
8388.930	2	4.09	−10.49	−49.9
8396.906	1	4.22	−3.29	–
8399.016	1	4.25	−2.32	–
8399.961	1	4.26	−1.98	–
8400.957	2	4.28	−1.78	−59.8
8401.902	2	4.29	−1.63	−55.8
8402.879	2	4.31	−1.64	−54.6
8403.965	2	4.33	−1.52	−53.5
8404.902	2	4.34	−1.56	−47.8
8406.945	2	4.37	−1.55	−50.1
8412.914	1	4.46	−1.70	–
8453.859	2	5.10	−11.04	−58.7
8455.883	2	5.13	−8.81	−57.8
8470.816	1	5.36	−1.62	–
8492.922	2	5.70	−1.50	–
8493.887	2	5.72	−1.59	−63.9
8500.875	2	5.83	−1.49	−57.4
8503.879	2	5.87	−1.44	−56.3
8504.883	2	5.89	−1.68	−53.8
8705.027	1	8.99	−2.36	–
8725.906	1	9.31	−1.73	–
8768.984	1	9.98	−1.44	–
8857.809	1	11.35	−1.14	–
8877.828	1	11.66	−4.20	–
8882.836	1	11.74	−2.31	–

© Royal Astronomical Society • Provided by the NASA Astrophysics Data System

1997MNRAS.286....1P

Table A4. Spectroscopic observations of AD Aql.

HJD	site	phase	W_λ	radial velocity	
				Hα ab	Hα em
2440000+		(ϕ)	(Å)	(km s^{-1})	(km s^{-1})
8389.219	2	4.58	−0.28	72.1	68.2
8401.145	2	4.76	+0.18	53.4	70.4
8403.094	2	4.79	+0.47	48.5	65.1
8407.219	2	4.85	+0.75	47.6	65.9
8454.070	2	5.56	+0.11	61.4	82.9
8494.016	2	6.16	+0.06	62.5	84.5
8500.035	2	6.25	+1.30	32.7	79.1
8501.098	2	6.27	+1.27	35.7	81.6
8503.070	2	6.30	+1.19	41.0	74.3
8507.023	2	6.36	+0.97	41.1	77.3
8509.109	2	6.39	+0.65	43.5	72.1

Table A5. Spectroscopic observations of V453 Oph.

HJD	site	phase	W_λ	radial velocity	
				Hα ab	Hα em
2440000+		(ϕ)	(Å)	(km s^{-1})	(km s^{-1})
8402.184	2	0.76	−0.76	−125.2	−129.0
8454.004	2	1.41	+0.74	−119.2	−123.1

Table A6. Spectroscopic observations of RY Ara.

HJD	site	phase	W_λ	Fe I rad. vel. 6546.245 Å
2440000+		(ϕ)	(Å)	(km s^{-1})
8346.078	1	0.11	+0.40	102.5
8397.254	1	0.28	+0.01	92.8
8401.113	2	0.30	−0.10	92.2
8401.180	1	0.30	−0.12	92.1
8407.047	2	0.32	−0.04	98.8
8412.074	2	0.33	−0.03	94.1
8453.977	2	0.48	−0.07	130.5
8470.875	1	0.54	−0.77	94.0, 131.0
8490.023	2	0.60	−0.53	112.5
8493.102	2	0.61	−0.39	107.4
8494.984	2	0.62	−0.39	113.3
8499.930	2	0.64	+0.02	107.9
8501.902	2	0.64	+0.03	113.8
8505.086	2	0.65	+0.10	107.8
8507.102	2	0.66	+0.21	113.5
8508.996	2	0.67	+0.13	109.3
8705.172	1	1.35	−0.10	99.1, 133.3
8725.141	1	1.41	+0.11	107.8
8769.148	1	1.57	−1.59	97.0, 125.3
8876.902	1	1.94	+0.40	120.5

Table A7. Spectroscopic observations of V820 Cen.

HJD	site	phase	W_λ	Fe I rad. vel. 6546.245 Å
2440000+		(ϕ)	(Å)	(km s^{-1})
8342.203	1	0.02	−0.00	−258.0
8386.980	2	0.30	−1.42	−259.4
8388.133	2	0.31	−1.54	−260.0
8388.992	2	0.32	−1.50	−258.5
8397.004	1	0.37	−1.09	−253.1
8399.063	1	0.38	–	−260.8
8400.020	1	0.39	−1.17	−259.0
8401.027	2	0.39	−1.31	−260.7
8403.027	2	0.40	−1.48	−255.4
8404.914	2	0.42	−1.39	−257.0
8453.949	2	0.72	−1.95	–
8455.906	2	0.74	−2.18	–
8466.895	1	0.80	–	−250.0
8469.930	1	0.82	−2.94	−250.1
8492.938	2	0.97	−2.64	−269.6
8494.938	2	0.98	−2.58	−264.9
8500.926	2	1.02	−2.31	−255.7
8502.922	2	1.03	−2.28	−258.0
8507.914	2	1.06	−1.98	−260.8
8508.980	2	1.07	−2.06	−261.5
8705.977	1	2.30	−1.67	−257.1
8706.098	1	2.30	−1.62	−259.1
8724.957	1	2.42	−1.63	−251.6
8767.961	1	2.69	−1.74	−260.7
8769.031	1	2.70	−1.72	−263.2
8877.867	1	3.38	−2.46	−250.0
8881.863	1	3.41	−2.20	−249.0

© Royal Astronomical Society • Provided by the NASA Astrophysics Data System

1997MNRAS.286....1P

Table A8. Spectroscopic observations of U Mon.

HJD	site	phase	W_λ	Fe I radial velocities		
				6200.321 Å	6750.164 Å	6546.245 Å
2440000+		(ϕ)	(Å)	(km s^{-1})	(km s^{-1})	(km s^{-1})
8286.969	1	1.70	−1.22	3.9	3.5	
8344.938	1	2.33	−1.12	25.2	25.0	
8346.836	1	2.35	−1.01	27.5	28.2	
8386.852	2	2.78	−1.92	–	–	5.2
8388.906	2	2.80	−1.88	–	–	12.3
8397.820	1	2.90	−1.51	30.8	31.0	
8401.848	2	2.94	−2.13	–	–	25.0
8405.852	2	2.99	−3.17	–	–	30.3
8471.285	1	3.70	−3.42	3.0	4.6	
8494.273	2	3.95	−4.32	–	–	37.3
8500.277	2	4.01	−5.90	–	–	50.0
8503.250	2	4.04	−6.78	–	–	53.8
8509.234	2	4.11	−7.38	–	–	52.4
8525.148	1	4.28	−3.09	20.2, 44.7	17.6, 46.4	
8526.219	1	4.29	−3.37	19.5	17.8, 46.0	
8575.066	1	4.82	−2.62	17.9	18.1	
8591.117	1	5.00	−4.78	–	–	40.3
8694.883	1	6.12	−5.56	50.5	48.6	
8704.840	1	6.23	−4.39	15.9, 51.8	13.8, 52.4	
8704.863	1	6.23	−4.39	14.7, 50.3	15.2, 51.4	
8722.906	1	6.42	−2.29	36.2	37.1	
8768.773	1	6.92	−1.72	29.3	29.3	
8856.262	1	7.87	−0.74	27.3	26.3	
8877.215	1	8.09	−3.02	54.1	50.7	
8878.246	1	8.11	−3.20	53.5	52.3	
8882.199	1	8.15	−2.78	12.9, 52.1	9.7, 51.1	
8883.207	1	8.16	−2.60	14.7, 53.2	15.3, 52.4	
8947.121	1	8.85	−0.65	26.1	26.0	
8949.074	1	8.87	−0.51	29.4	29.2	
9007.043	1	9.50	−0.78	47.2	49.8	
9033.887	1	9.79	−0.91	27.6	28.1	
9088.852	1	10.39	−0.60	34.1	34.4	
9227.270	1	11.89	−0.11	40.2	39.4	
9387.922	1	13.63	−1.90	19.9	19.9	
9389.887	1	13.65	−1.59	21.8	19.9	
9443.820	1	14.23	−0.26	35.5	33.9	
9446.852	1	14.26	−0.11	37.6	37.7	

Table A9. Spectroscopic observations of AI Sco.

HJD	site	phase	W_λ	Fe I radial velocity	
				6546.245 Å	6569.224 Å
2440000+		(ϕ)	(Å)	(km s^{-1})	(km s^{-1})
8402.070	2	0.40	4.32	−19.5	−16.3
8407.152	2	0.47	4.17	−1.9	−3.0
8412.082	2	0.54	3.82	+8.0	+7.3
8470.930	1	1.37	3.20	+0.4	−2.5
8490.035	2	1.64	1.20	−39.2	+16.0
8494.059	2	1.69	1.32	−30.0	−21.7
8499.953	2	1.77	1.52	−21.4	−20.8
8501.920	2	1.80	1.64	−20.2	−18.7
8505.098	2	1.85	1.89	−18.2	−15.4
8507.094	2	1.88	2.05	−10.3	−6.2

© 1997

© Royal Astronomical Society • Provided by the NASA Astrophysics Data System

1997MNRAS.286....1P

Table A10. Spectroscopic observations of AR Pup.

HJD 2440000+	site	phase (ϕ)	W_λ (Å)	C I rad. vel. 6587.622 Å (km s^{-1})
8346.875	1	3.55	−1.55	–
8386.867	2	4.06	−1.24	–
8388.887	2	4.09	−1.42	–
8397.875	1	4.20	−1.29	–
8399.859	1	4.23	−1.06	–
8401.859	2	4.25	−1.05	41.9
8402.875	2	4.27	−0.99	45.2
8404.879	2	4.29	−0.86	40.0
8410.820	1	4.37	−0.68	–
8494.230	2	5.44	−0.98	52.0
8500.227	2	5.52	−1.14	53.7
8503.230	2	5.56	−1.35	51.8
8509.219	2	5.63	−1.59	47.7
8494.098	1	6.72	−1.41	–
8695.012	1	8.02	−1.99	–
8704.898	1	8.15	−2.24	–
8768.816	1	8.97	−0.94	–
8878.199	1	10.38	−0.74	–
8883.172	1	10.44	−0.73	–

Table A11. Spectroscopic observations of IW Car.

HJD 2440000+	site	phase (ϕ)	W_λ (Å)	radial velocity Hα ab (km s^{-1})	radial velocity S I or C I (km s^{-1})
8344.988	1	3.08	0.97	+5.9	+7.8
8346.926	1	3.11	1.30	+2.5	+3.0
8386.879	2	3.67	2.76	–	+3.9
8388.914	2	3.69	2.71	–	−1.0
8397.926	1	3.82	1.64	−5.0	+6.9
8398.961	1	3.83	1.79	−10.8	−0.5
8399.910	1	3.85	1.78	−6.1	−5.1
8400.949	2	3.86	2.13	−3.3	+3.0
8401.898	2	3.87	2.57	−7.1	+3.1
8403.926	2	3.90	2.51	−6.8	+2.8
8404.887	2	3.92	2.40	−5.4	+5.5
8407.910	2	3.96	2.45	−8.2	+0.5
8453.848	2	4.60	2.68	−8.2	−11.0
8455.879	2	4.62	2.43	−10.1	−9.0
8467.832	1	4.79	1.86	−13.2	−7.7
8471.191	1	4.84	1.87	−21.4	−10.8
8472.195	1	4.85	2.15	−17.3	−5.1
8494.246	2	5.16	2.84	−20.5	−9.6
8500.242	2	5.24	3.03	−23.2	−9.0
8503.219	2	5.28	2.75	−26.9	−18.3
8509.203	2	5.36	3.30	−29.4	−17.3
8525.227	1	5.59	1.22	−32.4	−18.4
8526.180	1	5.60	1.47	−33.5	−15.6
8527.082	1	5.61	0.99	−31.4	−16.3
8576.129	1	6.29	1.24	−27.6	−18.9
8590.109	1	6.49	1.62	−26.3	−24.2
8494.961	1	6.56	1.65	−25.2	−24.2
8694.125	1	7.93	1.16	−29.6	−24.5
8705.094	1	8.09	1.32	−30.4	−24.1
8723.918	1	8.35	1.47	−26.8	−23.4
8767.867	1	8.96	1.34	−23.0	−21.7
8768.930	1	8.97	1.40	−22.9	−22.3
8878.082	1	10.49	2.13	−18.6	−27.2
8882.063	1	10.54	2.38	−20.5	−30.6
8883.098	1	10.56	1.98	−20.3	−30.6

This paper has been typeset from a TEX/LATEX file prepared by the author.

© Royal Astronomical Society • Provided by the NASA Astrophysics Data System